Geoscience Frontiers 16 (2025) 102017

Contents lists available at ScienceDirect

Geoscience Frontiers

journal homepage: www.elsevier.com/locate/gsf

Research Paper

A Mesoproterozoic missing link between eastern Australia and China during the transition from Nuna to Rodinia?

Alexander Edgar [a,b,*], Ioan Sanislav [a], Paul Dirks [a]

[a] College of Science and Engineering, Economic Geology Research Centre (EGRU), James Cook University, Townsville, Australia
[b] School of Earth Sciences – Centre for Exploration Targeting (CET), University of Western Australia, Perth, Australia

ARTICLE INFO

Article history:
Received 5 June 2024
Revised 20 January 2025
Accepted 17 February 2025
Available online 21 February 2025
Handling Editor: Mathew M. Domeier

Keywords:
Australia
China
Laurentia
Nuna
Rodinia
Mesoproterozoic
Tasmanides

ABSTRACT

We document, for the first time, Mesoproterozoic-aged, continental arc magmatism in the Tasmanides. Granitoid samples intruding the Proterozoic Cape River Metamorphics in northeast Queensland contain abundant ~ 1200 Ma igneous zircons, with early-Paleozoic metamorphic rim overgrowths. Analytical mixing between the igneous and metamorphic zircons produces cryptic discordant analyses, but the origin of said discordance is resolved with zircon Th/U ratios. Samples of the Fat Hen Creek Complex are peraluminous, calc-alkaline, S-type granitoids, that record high-grade metamorphism and trace element mobilization. The P3 and P42 intrusions are metaluminous, calc-alkaline, I-type granodiorite, which intruded the Cape River Metamorphics, and contain trace element signatures consistent with a continental-arc setting. We propose that a Mesoproterozoic continental terrane, herein referred to as the Oakvale Province, exists as basement to the Thomson Orogen. We propose several models for the formation of the Oakvale Province, with potential links to the Tarim Block, and the Yangtze Craton, during the late-Mesoproterozoic. We propose that the Oakvale Province supplied the Tasmanides with late-Mesoproterozoic detritus, and that such detritus was not solely sourced from the Musgrave Province as previously interpreted. Finally, we interpret the oroclinal bending of Paleozoic deformation and plutonic fabrics to reflect the buried extent of the Oakvale Province, and to potentially map out the Neoproterozoic rift margin associated with Rodinia break-up.

1. Introduction

The structure and evolution of the Australian lithosphere, within the context of Rodinia assembly and break-up, is a topic of uncertainty and debate. Two contested aspects of the Rodinia configuration are the position of Australia relative to Laurentia and several terranes of China, and the position of the east Australian rifted margin formed during Rodinia breakup. Many possible configurations have been proposed, however, a consensus has yet to be reached. Several authors have suggested that the eastern margin of the North Australian Craton (NAC), represented by the Mt Isa Inlier and Georgetown Inlier, records a Proterozoic history of suturing with the western margin of Laurentia during assembly of the Nuna supercontinent (Nordsvan et al., 2018; Pourteau et al., 2018; Volante et al., 2020a, 2020b, 2022). This connection has been proposed to have terminated during the transition from Nuna to Rodinia, with a period of late-Palaoproterozoic to Mesoproterozoic rifting and ocean basin development (Betts et al., 2016; Yang et al., 2023; Cao et al., 2024), followed by late-Mesoproterozoic to early-Neoproterozoic ocean-closure and re-assembly (Cao et al., 2024). Recent modelling by Cao et al. (2024) illustrates a substantial ocean basin separating Laurentia and Australia at ~ 1230 Ma. However, a late-Mesoproterozoic (1.3–1.0 Ga) detrital zircon signature within younger sedimentary successions of the Tasmanides (Blewett et al., 1998; Fergusson et al., 2001), may indicate active margin magmatism along eastern Australia during this time. Alternative models suggest that during the late-Mesoproterozoic, the core of Rodinia consisted of the eastern margin of the NAC and various tectonic elements of China, including the Yangtze Craton (Li et al., 2002, 2008) or the Tarim Block (Wen et al., 2017, 2018). The Mesoproterozoic was a key interval for the assembly of the Yangtze Craton-Cathaysia (Greentree et al., 2006; Li et al., 2007), and the Tarim Block composite terranes (Wang et al., 2021), and geographic proximity to eastern Australia during the late-Mesoproterozoic may increase the likelihood of shared history between the terranes.

* Corresponding author at: College of Science and Engineering, Economic Geology Research Centre (EGRU), James Cook University, Townsville, Australia.
E-mail address: Alexander.edgar@my.jcu.edu.au (A. Edgar).

https://doi.org/10.1016/j.gsf.2025.102017

In this contribution, we present new geochronological and geochemical data from intrusive rocks collected from the Cape River Metamorphics, north Queensland, Australia. These intrusive rocks represent the oldest intrusions recorded within the Tasmanides, and suggest the presence of a concealed, Proterozoic terrane, beneath the Thomson Orogen. We suggest that this continental terrane may have collided with the North Australian Craton during the transition from Nuna to Rodinia in the Mesoproterozoic. Our interpretation provides crucial constraints on Australia's position within Nuna-Rodinia configurations, and thus, we present new models depicting the tectonic evolution of the east Australian margin during the Mesoproterozoic.

2. Geological context

Assembly of the Rodinia supercontinent has been recorded globally by numerous Mesoproterozoic-Neoproterozoic orogenic belts. In Australia, late-Mesoproterozoic orogenesis has been documented within several mobile belts including the Albany-Fraser Orogen, Capricorn Orogen, and Musgrave Province (Clark et al., 2000; Sheppard et al., 2007; Aitken and Betts, 2008; Smits et al., 2014). These mobile belts record the Proterozoic amalgamation of Australia through suturing of the NAC, South Australian Craton (SAC) and West Australian Craton (WAC).

During the Neoproterozoic, rifting, associated with the breakup of Rodinia, has been recorded within the Adelaide Superbasin (Powell et al., 1994; Preiss, 2000; Lloyd et al., 2020, 2022), and extrapolated northwards running parallel to the eastern margin of cratonic Australia. By the late-Neoproterozoic – early-Paleozoic, rifting in eastern Australia, which was positioned along the eastern margin of Gondwana, was terminated by the onset of convergent tectonics (Cawood, 2005; Foden et al., 2020). Neoproterozoic-Paleozoic convergent tectonics along the eastern and southern margins of Gondwana have been attributed to the Terra Australis Orogen. The Terra Australis Orogen was a long-lived, accretionary-style subduction system, and is widely cited as the type-example of such a system (Cawood, 2005; Cawood et al., 2009). Interpretations of Wilson cycle-style tectonics have been mostly rejected for the Terra Australis Orogen.

Along the northeastern margin of Gondwana, the evolution of the Terra Australis Orogen has been recorded by the Tasmanides (Glen, 2005; Rosenbaum, 2018). The Tasmanides comprise a tectonic collage of Neoproterozoic-Paleozoic orogens that have been interpreted to record an accordion-style of tectonics. This tectonic regime involved cyclical opening and inversion of extensive back-arc basin successions in response to a westward dipping, Andean-style subduction margin. The largest, and most poorly understood of these orogens is the Thomson Orogen, which is largely concealed by Mesozoic sedimentary cover of the Great Artesian Basin (Purdy et al., 2016, 2018). A feature of Neoproterozoic-Paleozoic *meta*-sedimentary successions throughout the Thomson Orogen is a late-Mesoproterozoic, detrital zircon signature. This detritus was thought to be derived from a source within the Musgrave Province (Fergusson and Henderson, 2015; Purdy et al., 2016).

Along its margins, exposures of the Thomson Orogen basement preserve evidence of Delamarian-aged deformation (Abdullah et al., 2020; Dirks et al., 2021). This deformation, and subsequent deformation events, have resulted in a regional-scale deformation and plutonic fabric, which wraps around the margins of the Thomson orogen. Along the northern and southern margins, this fabric predominantly strikes east–west orientation, and along the eastern margin, it is oriented north–south.

In north Queensland, rocks of the Thomson Orogen are best exposed within the Charters Towers Province. The Charters Towers Province contains numerous exposures of basement metamorphic rocks, including the Running River Metamorphics (Dirks et al., 2021; Edgar et al., 2022, 2023), Argentine Metamorphics (Fergusson et al., 2007a, 2007b), Cape River Metamorphics (Fergusson et al., 2005) and Charters Towers Metamorphics (Fig. 1A). Extending along the western margin of the Charters Towers Province, the Cape River Metamorphics form a northwest-southeast trending belt of moderately to strongly deformed, *meta*-sedimentary and *meta*-igneous rocks (Fig. 1B). The easternmost Cape River Metamorphics comprise lensoidal exposures of amphibolite juxtaposed within undifferentiated quartzose schist and felsic gneiss belonging to the Cape River Beds. In the west, the Cape River Metamorphics consist mostly of the Morepork Member, which is composed of a series of interbedded quartzite ridges, metasandstone and graphitic schist (Fergusson et al., 2005; Henderson et al., 2020). The Fat Hen Creek Complex intruded the Cape River Beds (Blewett et al., 1998; Fergusson et al., 2005), and consists of deformed granitoids, orthogneiss and migmatite. Henderson et al. (2020) interpreted the Cape River Metamorphics as a conformable *meta*-sedimentary sequence deposited within an early-Paleozoic back arc-basin. Northeast-southwest oriented compression during the Silurian-Devonian folded the Cape River Metamorphics into a northwest-southeast trending syncline, with the Morepork Member in its core (Fergusson et al., 2005).

The Morepork Member metasediments contain both 650–500 Ma and 1.3–1.0 Ga detritus. However, outside of the Morepork Member, the 650–500 Ma detritus is absent, and the prominent 1.3–1.0 Ga signature dominates (Henderson et al., 2020). The lack of 650–500 Ma zircons within the Cape River Beds may suggest that a previously unrecognized unconformity separates the Cape River Beds and Morepork Member. Therefore, metasediments belonging to the Cape River Beds, which were deposited below the unconformity, are probably unrelated to a Paleozoic back arc basin infilled by 650–500 Ma sediment as previously interpreted (Henderson et al., 2020).

3. Methods

Fieldwork was conducted within Oakvale Station, which is situated ~ 30 km northwest of the township of Pentland. The main aim of the fieldwork was to sample intrusive rocks situated below the interpreted unconformity separating the Morepork Member and Cape River Beds. These samples would be used to constrain the age of the Cape River Metamorphics, and to ascertain the geochemical character of intrusive rocks in the region. Four samples of the P42 Intrusion, two samples of the P3 Intrusion, one sample of the Fat Hen Creek Complex (FHCC), one sample of the mylonitised FHCC (FHCC mylonite), and one sample of migmatite (P16 migmatite) were collected for geochronological and geochemical analyses (Fig. 1B).

Zircons grains were separated from each sample using rock crushing, Wilfley table heavy mineral separation, and handpicking of zircon grains. Zircon grains were mounted in epoxy pucks for cathodoluminescence imaging on a Jeol JSM5410LV SEM hosted within the Advanced Analytical Centre at James Cook University. Zircon U-Pb isotopes and trace elements (U, Pb, Th) were measured using the GeoLas 200 Excimer laser ablation system combined with a Varian ICPMS 820 series instrument. Laser conditions were set at 3 J/cm^2 with a spot size of 20 μm. The zircon standard GJ1 was used as a primary standard, and zircon standards TM1, Plesovice, Temora 2, and 91500 were used as secondary standards. NIST610 glass was analysed at the start and end of each sample run to correlate $^{207}Pb/^{206}Pb$ ratios. Zircon rims were targeted during analyses to determine the magmatic crystallization age. Raw data reduction was primarily processed using Iolite 4 software with further data processing performed on Isoplot R software.

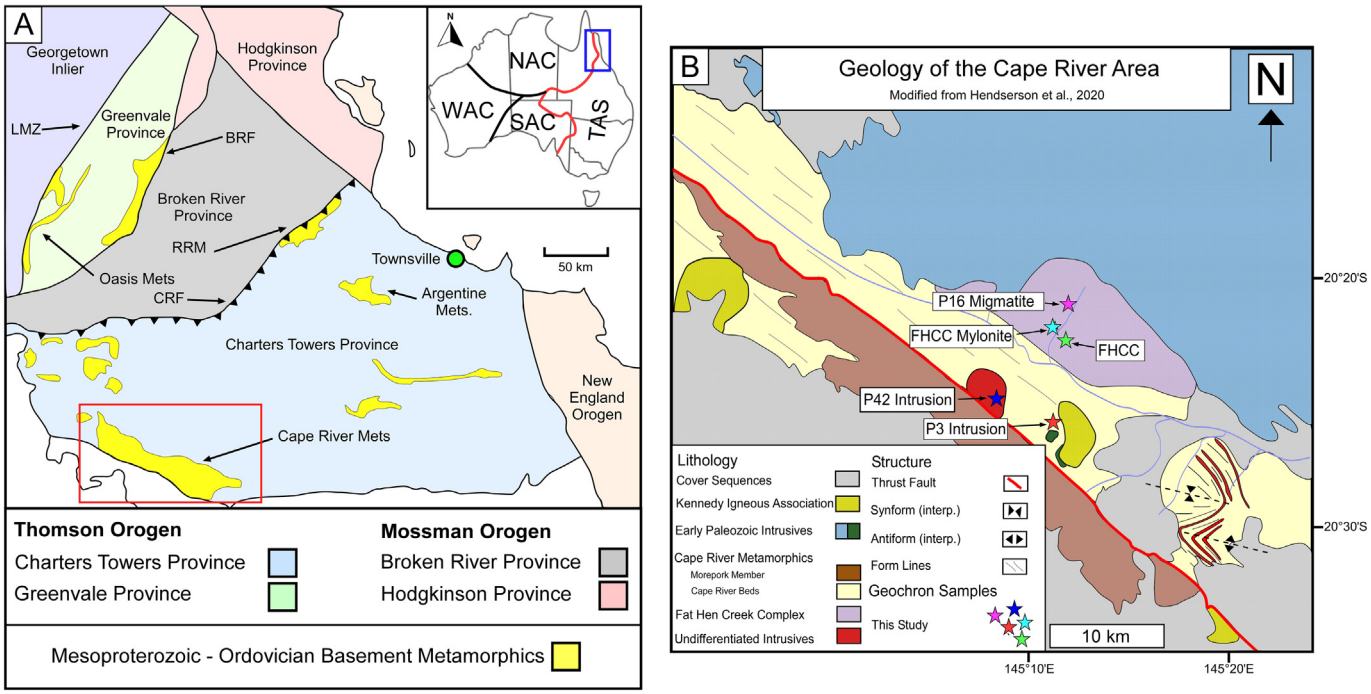

Fig. 1. (A) Paleozoic tectonic framework of northeast Queensland. Location of the Cape River Metamorphics highlighted by the red square. The inset map illustrates a simplified configuration of the main tectonic components of Australia for reference. (B) Geological map of the Cape River Metamorphics, modified from Henderson et al. (2020). NAC, North Australian Craton; WAC, West Australian Craton; SAC, South Australian Craton; TAS, Tasmanides; LMZ, Lynd Mylonite Zone; BRF, Burdekin River Fault; RRM, Running River Metamorphics; CRF, Clarke River Fault.

Whole-rock major elements were analysed for eight samples using SEM-EDS. Trace elements were analysed for the same eight samples using the ICP-OES, with Al concentrations, ascertained from earlier EDS analysis, used as the internal standard. The trace element composition of each sample was analysed three times (See Supplementary Materials) for a total of twenty-four trace element analyses.

4. Lithological descriptions

4.1. The P3 Intrusion

The P3 Intrusion (Fig. 2A) is an unaltered, medium grained, equigranular, *meta*-granite. It is composed mostly of quartz, plagioclase, and orthoclase, with accessory magnetite, and contains a prominent lineation defined by stretched feldspars. The P3 Intrusion is exposed in a small gully outcrop, where it crosscuts the low-grade metapelites of the Cape River Beds at a high angle, and it is intruded by a thin, undeformed, basaltic dyke.

4.2. The P42 Intrusion

The P42 Intrusion (Fig. 2D) was identified in aerial photography as a 25 km^2, dome shaped intrusive body consisting of northwest trending ridges interpreted to reflect foliation. The P42 Intrusion is a medium grained, equigranular granitoid, comprised of quartz, feldspar, and hornblende. The intrusion is progressively more deformed from core to rim. In its core, the P42 Intrusion preserves an igneous texture and contains a variably developed mineral lineation best defined by the alignment of hornblende. Along it's margins, the P42 Intrusion has been intensely deformed into a gneiss a with foliation that parallels the regional northwest trending fabric. The exact contact of the intrusion with the surrounding metasediments can be difficult to determine, due to the intensity of the deformation. The P42 Intrusion is crosscut by late, quartz-epidote veins that were best developed within pre-existing foliation planes.

4.3. The Fat Hen Creek Complex

Samples of the Fat Hen Creek Complex (FHCC) consists of a coarse-grained granite, comprised mostly of biotite, quartz and feldspar (Fig. 2C). The granite has been observed at several outcrops within the FHCC, however, contacts to the surrounding rock types are commonly concealed. This biotite-rich granite probably comprises the bulk of the mapped Fat Hen Creek Complex (Fig. 1B) and has been intruded by several felsic intrusions belonging to the Siluro-Devonian Lolworth Suite. The FHCC contains xenoliths of deformed metasediment and amphibolite.

4.4. The Fat Hen Creek Complex mylonite

The Fat Hen Creek Complex is crosscut by a series of ductile shear zones which have formed a localized proto-mylonitic variant of the Fat Hen Creek Complex granite (Fig. 2B). It is distinct in composition from the typical FHCC granite, consisting mostly of coarse-grained biotite and megacrystic feldspar porphyroclasts, with lesser quartz, and minor garnet and opaques.

4.5. P16 migmatite

The P16 migmatite was observed in several subcrops and as boulder-sized float within the FHCC. The P16 migmatite consists of coarse laminations of amphibole-rich melanosome and quartzo-feldspathic leucosome (Fig. 2E). The sample obtained for zircon U-Pb dating was collected from the leucosome fraction of the migmatite, and consists of coarse-grained quartz, plagioclase, and biotite. The leucosome fraction of the migmatite contains a pronounced stretching lineation defined by biotite. The full extent

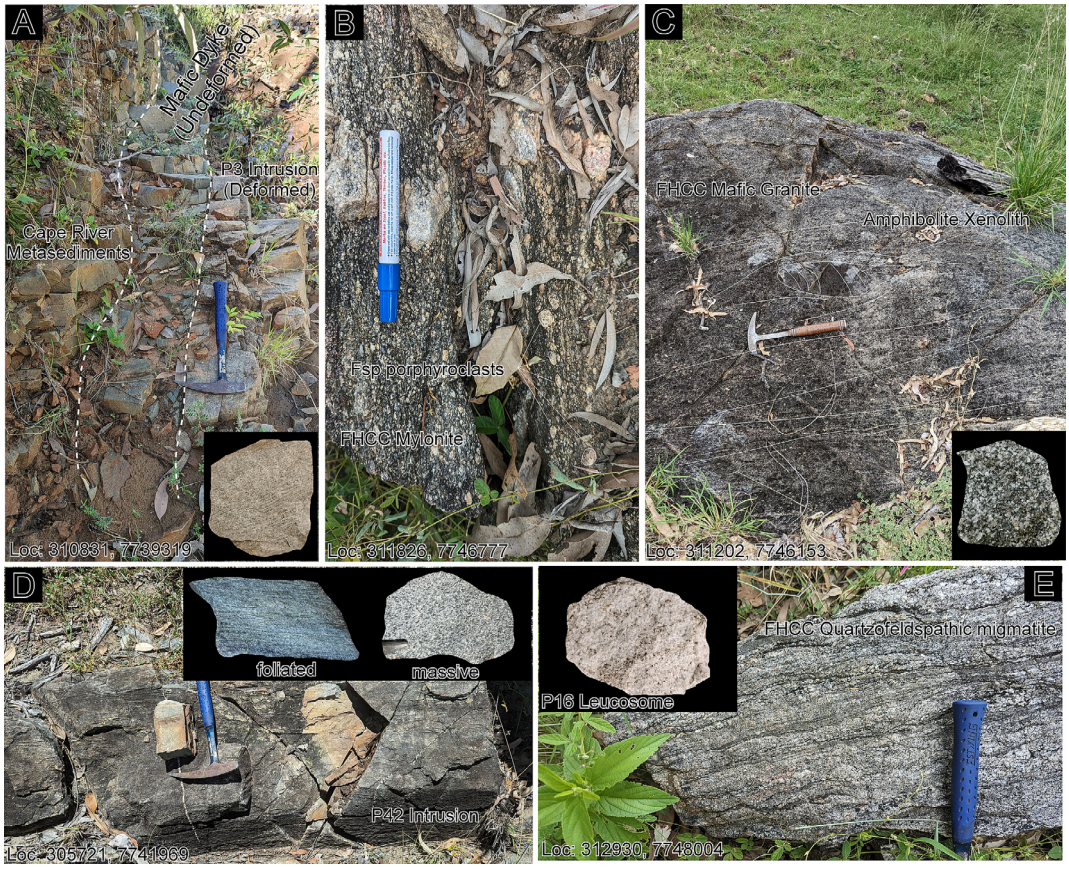

Fig. 2. Field photographs of key outcrops sampled during fieldwork on Oakvale Station. (A) Creek bed outcrop of the P3 Intrusion, which has intruded interbedded metasandstone-schist units of the Cape River Metamorphics. The contact of the P3 Intrusion and Cape River Metamorphics was later intruded by an undeformed mafic dyke. (B) Mylonite of the Fat Hen Creek Complex which contains coarse-grained feldspar porphyroclasts. (C) Typical, massive, coarse-grained, biotite-rich granite of the Fat Hen Creek Complex which contains xenoliths of folded amphibolite and metasediments. (D) Foliated and massive varieties of the P42 Intrusion. Intensely foliated varieties, observed within high strain zones along pluton margins, could be easily mistaken for laminated metasediments. Weakly deformed varieties of the P42 Intrusion, with an original igneous texture, were sampled from within the core of the intrusive body. (E) Subcropping laminated migmatite comprising bands of quartzo-feldspathic leucosome and amphibole-rich melanosome. The P16 Migmatite sample was collected from quartzo-feldspathic leucosome fraction.

and distribution of migmatite within the FHCC has not been constrained.

5. Geochronology

Five samples, one from each of the rock types described, were selected for U/Pb zircon dating, with locations of the samples shown in Fig. 1B. Zircon rims were the focus of the analyses. The samples generally display a significant discordant population of analyses (discussed in *The origin of zircon discordance* below). For consistency, we have used discordia upper intercept ages, and weighted mean ages for final age determination (Fig. 3). Errors are reported as 2 sigma (2σ) propagated uncertainties.

5.1. The P3 Intrusion

Zircon grains from the P3 Intrusion are generally of subhedral form and typically display thin overgrowth zones around igneous and inherited cores. In CL, the grains are generally concentrically zoned with variable luminescent response. Sixty-seven analyses of zircon grains from the P3 Intrusion were collected. Most of the grains in the sample are discordant (See Supplementary Data for full results) but a population of twelve grains are clustered close to concordia. This near concordant population can be plotted along a discordia which produces an upper intercept age of 1209 ± 9 Ma. The weighted mean of the twelve near concordant analyses is also 1209 ± 9 Ma (MSWD = 0.51) (Fig. 3). The combined weighted mean age and discordia age of ~ 1209 Ma is interpreted to represent the intrusive age of the rock. Zircons from the P3 Intrusion contain an average Th/U ratio of 0.78.

5.2. The P42 Intrusion

The P42 Intrusion contains euhedral, prismatic zircons, that display low level luminescence in CL imaging. Due to the lack of luminescence, the P42 Intrusion zircons were imaged under secondary electron microscopy to scan for imperfections and mineral inclusions. Thirty-nine analyses were collected for zircons from the P42 Intrusion. Similar to zircon grains collected from the P3 Intrusion, most analyses were discordant (Supplementary Data for full results), but a cluster of eleven, mostly concordant, grains produced a discordia upper intercept age of 1172 ± 16 Ma. The weighted mean of the same population is 1174 ± 10 Ma (MSWD = 0.81) (Fig. 3). The weighted mean age of the sample of ~ 1174 Ma is interpreted to be the intrusive age of the rock. Zircons from the P42 Intrusion contain an average Th/U ratio of 0.68.

5.3. The Fat Hen Creek Complex (FHCC)

The FHCC granite contains euhedral zircons with low aspect ratios. The zircon grains typically comprise a strongly luminescent core, surrounded by a thick, weakly luminescent overgrowth. Con-

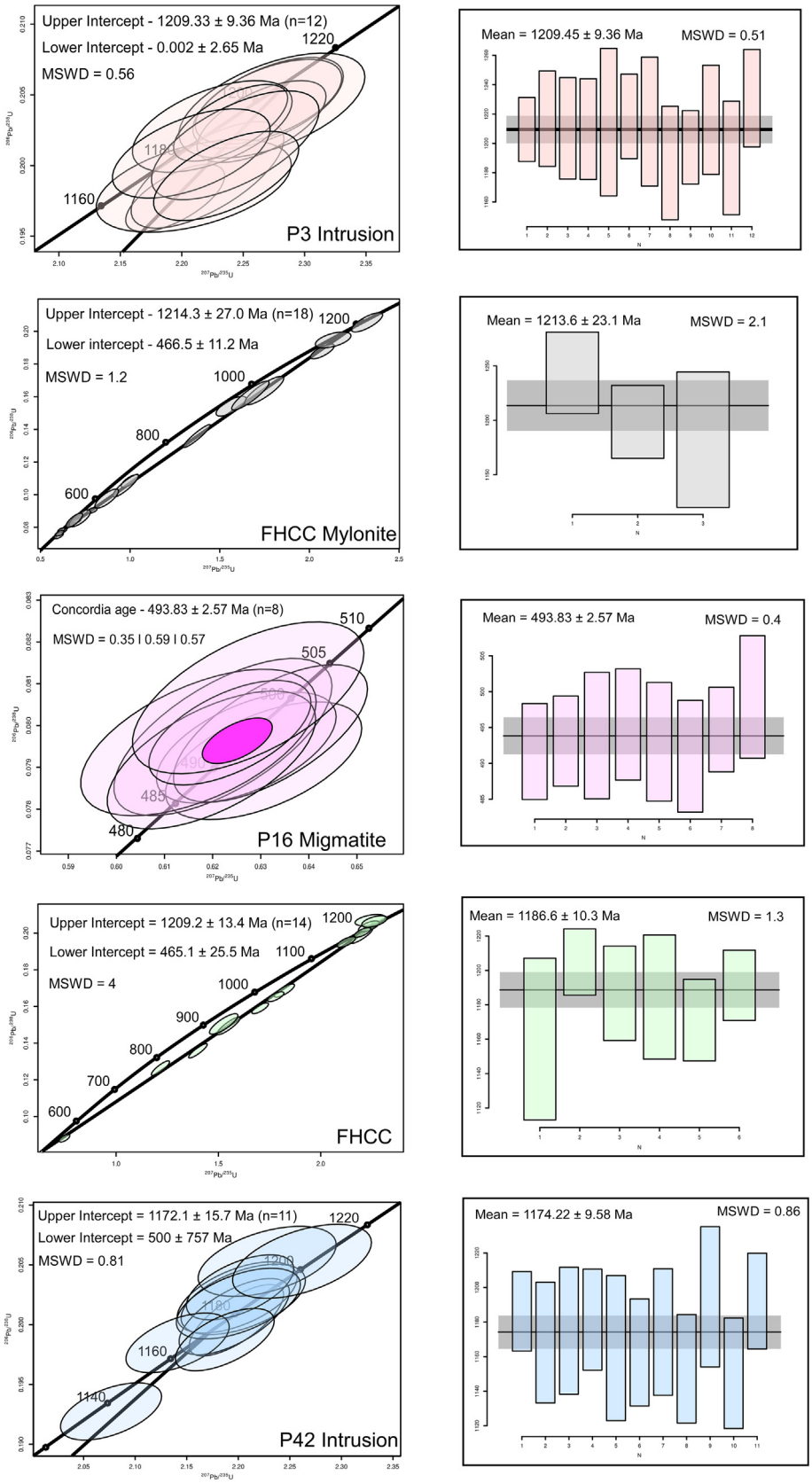

Fig. 3. Compilation of concordia plots and weighted mean plots from U/Pb geochronology of zircons from intrusions in the Cape River Metamorphics. Red – P3 Intrusion, grey – FHCC Mylonite, magenta – P16 migmatite, green – FHCC granite, blue – P42 Intrusion.

centric zonation is commonly discontinuous between the core and overgrowth zones (Fig. 3). Fifty-four analyses of the FHCC granite zircons were collected. The results display a clear linear discordant trend defined by fourteen analyses. The discordia line produced an upper intercept age of 1209 ± 13 Ma, and lower intercept of 465 ± 26 Ma, however, the lower intercept age is constrained by a single. A cluster of six concordant grains produced a weighted mean age of 1186 Ma ± 10.3 (MSWD = 1.3) (Fig. 3). The discordia upper intercept age of ~ 1209 Ma is interpreted as the intrusive age of the rock. Zircons from the FHCC granite contain an average Th/U ratio of 0.45.

5.4. The Fat Hen Creek Complex mylonite

Zircon grains contained within the FHCC mylonite are morphologically similar to those in the FHCC granite, characterized by luminescent cores and thick overgrowth zones. Forty-three analyses for zircon grains from the FHCC mylonite were collected. The results are comparable to the FHCC granite, with a discordia defined by eighteen grains. Many analyses of zircons from the FHCC Mylonite plotted towards the lower intercept of concordia at 467 ± 11 Ma, whilst only three analyses plotted close to the upper intercept of 1214 ± 27 Ma. The three analyses which plotted close to the upper intercept produced a weighted mean age of 1214 ± 23 Ma (MSWD = 1.2) (Fig. 3). The discordia upper intercept age of ~ 1214 Ma is interpreted as the intrusive age of the rock. Zircons from the FHCC mylonite contain an average Th/U ratio of 0.23.

5.5. P16 migmatite

Zircons extracted from the P16 migmatite are morphologically and chemically unique. The grains are euhedral with large aspect ratios, low luminescence, and they display no distinctive cores and rims. Sixty analyses of zircons from the migmatite were collected, with most analyses plotting discordantly. Eight concordant grains produced a concordia age and mean weighted age of 494 ± 3 Ma (MSWD = 0.4) (Fig. 3). The migmatite sample did not contain any pre-Cambrian concordant or discordant grains. This is a unique feature of the migmatite. All previously reported samples contain a significant Mesoproterozoic component. We interpret the mean weighted age of ~ 494 Ma as the age of migmatite crystallization. Zircons from the P16 migmatite contain an average Th/U ratio of 0.03.

6. Zircon Hf isotopes

Ablation sites for Hf isotope analyses were selected atop previously analysed U-Pb isotope analysis spots which yielded concordant results in samples of the P3 Intrusion, FHCC mylonite, and P16 migmatite. The aim of the Hf isotope analyses was to fingerprint whether Precambrian and Paleozoic zircon grains contained distinct Hf isotopes compositions relating to differing magmatic provenance. Laser ablation Hf isotope analyses for zircon grains were performed in the Advanced Analytical Centre at James Cook University, using a GeoLas 193-nm Arf-Laser Thermo-Scientific Neptune MC-ICP-MS.

A total of 34 Hf spot analyses for zircon were collected from the P3 Intrusion zircons (17 analyses), FHCC mylonite zircons (9 analyses) and P16 migmatite zircons (8 analyses). Zircons from the P3 Intrusion record a wide range of $\varepsilon_{Hf}(t)$ values of +9.6 to −11.8 and calculated model ages ranging between 1491 Ma and 2144 Ma. Zircons from the FHCC mylonite dominantly comprise strongly negative epsilon Hf values within the range of +1.2 to −32 and calculated model ages range from 1589 Ma to 2321 Ma. Zircons from the P16 migmatite yield a tight spread of negative $\varepsilon_{Hf}(t)$ values ranging between −6.2 and −8.7 with tightly constrained model ages between 1357 Ma and 1429 Ma.

7. Whole rock geochemistry

Whole rock geochemistry was obtained for all eight samples described in the methods section. The full tabulated major and trace-element geochemistry has been listed in the Supplementary Data.

7.1. The P3 and P42 intrusions

The P3 Intrusion and P42 Intrusion are geochemically alike. They contain 64–69 wt.% SiO_2, 9–13 wt.% Al_2O_3, 5–9 wt.% CaO, 1.8–3.3 wt.% Na_2O, 1.5–4.2 wt.% K_2O, 3.6–5.8 wt.% FeO, 2.3–3.8 wt.% MgO, and 0.6–1.0 wt.% TiO_2. The P3 Intrusion recorded ~ 3 wt.% LOI, whilst the P42 Intrusion recorded 0.7–1.4 wt.% LOI. Both intrusions are granodioritic in composition (Fig. 4A), with metaluminous (Fig. 4B), calc-alkaline geochemical affinities (Fig. 4C), which plot within the mantle fractionate field of Batchelor and Bowden (1985) (Fig. 4D). The intrusions fall within the volcanic-arc fields in trace element discrimination plots after Pearce et al. (1984) (Fig. 5A, B). In chondrite-normalized REE plots (Fig. 5C), the P3 and P42 intrusions display negative Eu anomalies, and LREE/HREE enrichment. Both intrusions share similar chondrite- normalized trace element compositions, with distinctly negative Nb and Ta anomalies (Fig. 5D).

7.2. The Fat Hen Creek Complex granite and mylonite

The samples of mafic granite from the Fat Hen Creek Complex are geochemically distinct from each other, and the P3 and P42 intrusions. The FHCC mafic granite sample contains 57 wt.% SiO_2, 16.5 wt.% Al_2O_3, 1.7 wt.% CaO, 2 wt.% Na_2O, 4.5 wt.% K_2O, 11.4 wt.% FeO, 3.8 wt.% MgO, and 1.4 wt.% TiO_2. The FHCC mafic granite recorded 1.2 wt.% LOI. The FHCC mylonite contains 68 wt.% SiO_2, 12.7 wt.% Al_2O_3, 1.8 wt.% CaO, 1.7 wt.% Na_2O, 5.1 wt.% K_2O, 7 wt.% FeO, 2.4 wt.% MgO, and 1.1 wt.% TiO_2. The FHCC mylonite recorded 0.5 wt.% LOI. The FHCC mafic granite is monzonitic in composition, whilst the mylonite is classified as a granodiorite (Fig. 4A). Both FHCC samples are weakly peraluminous – peraluminous in character (Fig. 4B) and plot within the calc-alkaline field of Th/Yb vs Zr/Y discrimination figure after Ross and Bédard (2009) (Fig. 4C). In the R1-R2 discrimination plot after Batchelor and Bowden (1985), the FHCC mafic granite falls within the *syn*-collision field, whilst the FHCC mylonite plots within the late orogenic field (Fig. 4D). The FHCC samples plot inconsistently within the tectonic discrimination plots of Pearce et al. (1984) falling across the *syn*-collisional, within-plate, and volcanic-arc fields (Fig. 5A, B). In the chondrite-normalized REE plot, both FHCC samples record negative Eu anomalies, whilst the FHCC mylonite records a distinct HREE depletion relative to the FHCC mafic granite (Fig. 5C). Both intrusions display sharply negative Sb and Mo, with moderately negative Nb, and weakly negative Ta anomalies (Fig. 5D).

8. Discussion

8.1. The origin of zircon discordance

Discordant analyses in zircon U/Pb geochronology have been commonly interpreted to reflect Pb-loss (Mezger and Krogstad, 1997). Zircon grains in rocks exposed to high-grade metamorphic conditions may record complete or partial resetting of their U-Pb decay system (Ashwal et al., 1999; Giacomini et al., 2005;

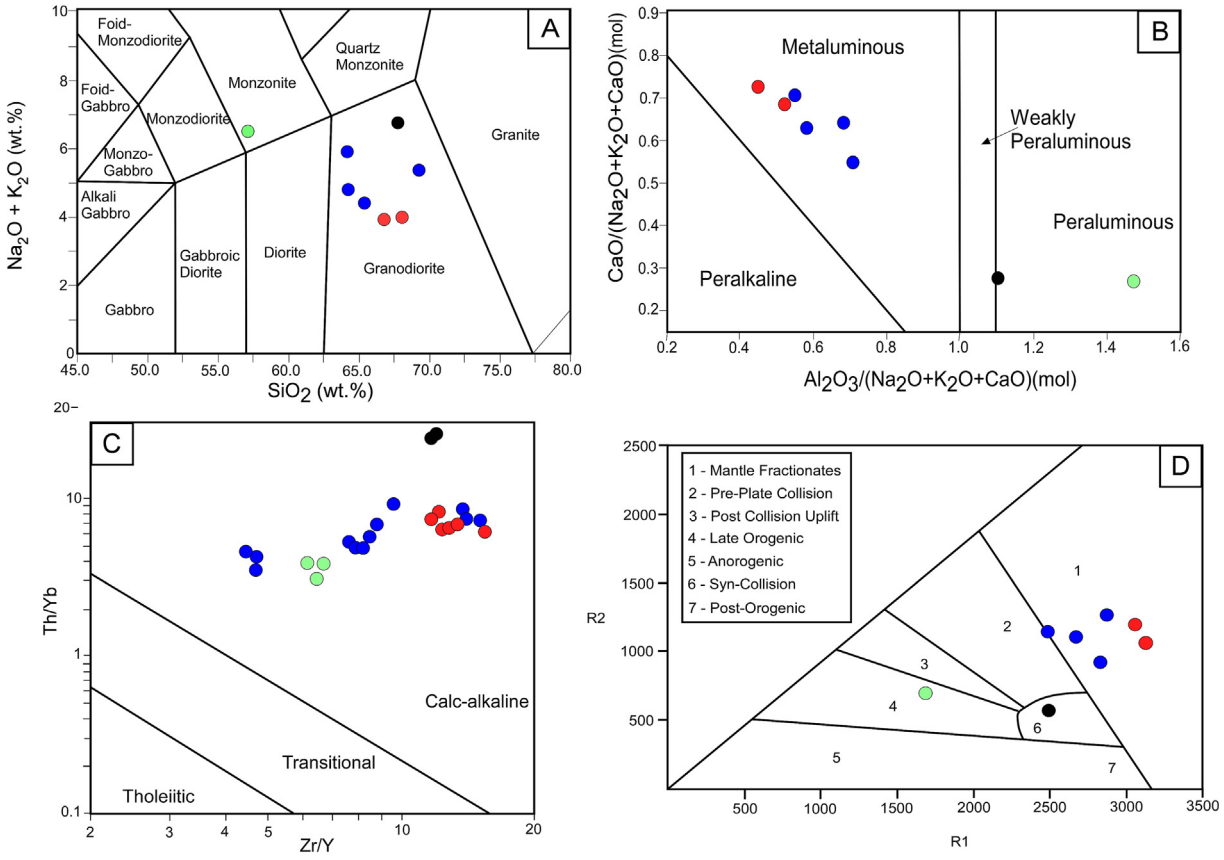

Fig. 4. Compilation of major and trace element geochemical discrimination plots. P3 Intrusion – red, P42 Intrusion – blue, FHCC granite – green, FHCC mylonite – black. (A) Total alkalis vs SiO_2 discrimination plot for igneous rock classification after Middlemost (1994). (B) Alumina saturation in igneous rocks after Barton and Young (2002). (C) Th/Yb vs Zr/Y magmatic affinity discrimination plot after Ross and Bédard (2009). (D) R1-R2 discrimination diagram after Batchelor and Bowden (1985). R1 is equal to 4Si – 11 (Na + K) – 2(Fe + Ti), R2 is equal to 6Ca + 2 Mg + Al.

Flowers et al., 2010; Wan et al., 2011; Rubatto, 2017). Contrarily, numerous studies have reported a lack of U-Pb system modification under high-grade crustal conditions (Hölttä et al., 2000; Carson et al., 2002; Kooijman et al., 2011). Besides metamorphism or alteration, discordance can reflect analytical mixing, whereby multiple generations of zircons are ablated during a single analysis (Spencer et al., 2016; Vervoort and Kemp, 2016). The U/Pb system of each zircon generation becomes contaminated by one another, and when viewed on a concordia plot, this contamination produces a mixing line that extends between the ages of each generation (Amelin et al., 2000; Vervoort and Kemp, 2016).

It is common in high-grade metamorphic terranes for new zircon crystals to preferentially nucleate upon pre-existing zircon, producing overgrowth zones of chemically and isotopically distinct zircon (Chen et al., 2010; Rubatto, 2017; Yakymchuk et al., 2018). In such scenarios, the Th/U ratio of zircon is a useful tool in discriminating igneous zircon (>0.1 Th/U) from metamorphic zircon (<0.1 Th/U) (Yakymchuk et al., 2018). On average, zircons from the P3 Intrusion and P42 Intrusion contain a significantly higher ratio of Th/U than the FHCC samples (Fig. 6). Zircons from the P16 migmatite, which yield an early-Paleozoic age of ~ 490 Ma, contain the lowest Th/U ratios (Th/U = 0.03) and are clearly of metamorphic origin. The metamorphic age returned by the P16 migmatite is within error of the lower discordia intercepts calculated for the FHCC samples (Fig. 3). This suggests that the discordant analyses obtained from zircons in the FHCC samples resulted from the influence of metamorphic zircon precipitation at ~ 490 Ma. This is consistent with the development of thick overgrowth zones within zircons from the FHCC samples, particularly within zircons from the FHCC mylonite (Fig. 6). This is further supported by the lack of early-Paleozoic age results in the P42 Intrusion and P3 Intrusion, which record lower-grade metamorphism and do not show evidence of migmatisation.

The origin of the discordant chronology trends (Fig. 3), which are particularly prominent in samples from the FHCC granite, are hereby attributed to mixed sampling of igneous zircon "cores" and metamorphic zircon overgrowths. During this study, ablation sites for U/Pb zircon geochronology were prioritized at grain boundaries, as this spot placement was considered most optimal for obtaining an accurate igneous crystallization age of the intrusive rock samples. However, in samples from the FHCC granite, where the metamorphic grade is high, and zircon grains have developed thick overgrowths, ablation spots positioned within zircon rims were likely to ablate both the primary zircon and the overgrowth, producing mixed analyses. The analytical signal produced by this contamination process is presented in Fig. 7, which illustrates the change in Th/U ratio and the resultant $^{206}Pb/^{238}U$ age produced during a single analysis of zircon from the FHCC granite. In the early stages of the analysis, the ablated zircon material contains a low Th/U ratio, and a resultant $^{206}Pb/^{238}U$ age of ~ 500 Ma, consistent with a zone of early-Paleozoic metamorphic zircon. As the analysis proceeds, the Th/U ratio sharply increases, and the resultant $^{206}Pb/^{238}U$ age changes accordingly to ~ 1200 Ma. This indicates a period when the ablation of dominantly early-Paleozoic metamorphic zircon switches to dominantly Mesoproterozoic igneous zircon, which we interpret as the igneous crystallization age of the rock. In Fig. 7, the inset concordia plot illustrates how time selection time influences the final age deter-

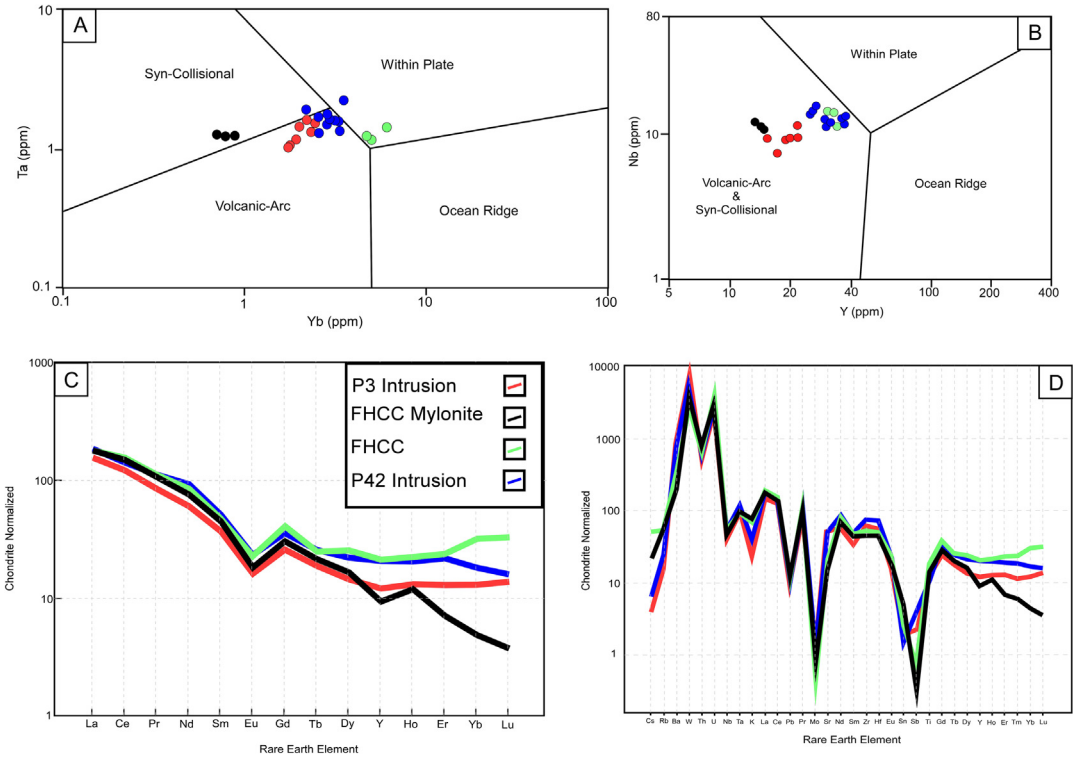

Fig. 5. Compilation of trace element discrimination and normalisation plots. P3 Intrusion – red, P42 Intrusion – blue, FHCC granite – green, FHCC mylonite – black. (A & B) Trace element discrimination of tectonic setting after Pearce et al. (1984). (C & D) Chondrite-normalized trace element spider diagrams. Normalizing values from McDonough and Sun (1995).

mination. If the first ~ 10 s of the full analysis is selected, the result plots concordantly at ~ 500 Ma. If the final ~ 10 s of the full analysis is selected, the result plots concordantly at ~ 1200 Ma. If the whole analytical time is selected, the result plots along a discordia line that intersects concordia at ~ 500 Ma and ~ 1200 Ma. This discordia line can be considered as a mixing line between the two generations of zircon; an earlier, Mesoproterozoic, generation of igneous zircon, and a later, early-Paleozoic, generation of metamorphic zircon.

Previous geochronological investigations by Henderson et al. (2020) and Fergusson et al. (2007a), Fergusson et al. (2007b) have interpreted that the Cape River Metamorphics were deposited within a Neoproterozoic to early-Paleozoic back-arc basin. This interpretation was largely based on detrital zircon geochronology results of metapsammitic rocks collected from the Morepork Member, and metapelites collected of the Cape River Beds. Samples CR190 (Fergusson et al., 2007a, 2007b) and CRA1 (Henderson et al., 2020) were sampled from the Morepork Member, and contain significant Neoproterozoic detrital zircon populations. Samples CRA2, CRA3, and IWH043 were collected from the Cape River Beds, and notably, to the east of the thrust contact between the Morepork Member and Cape River Beds (Fig. 1B). The samples collected from the Cape River Beds show a marked difference in their detrital zircon composition, and are notably lacking in Neoproterozoic detritus, except for a single, early-Paleozoic grain in CRA2 (Fergusson et al., 2007a, 2007b; Henderson et al., 2020). Additionally, sample CRA2 yielded four age dates between 1011 Ma and 1021 Ma, and this sample, described as a *meta*-arenite, was collected from within the P42 Intrusion. CRA2 may have been collected from the higher strain domains that encompass the P42 Intrusion, which consist of an intense, finely laminated compositional foliation (Fig. 2D), and is difficult to distinguish from the laminated metasediments of the Cape River Beds which it intruded.

Zircon U-Pb dating of the intrusive Fat Hen Creek Complex presented in Henderson et al. (2020) for sample LHL0228 yielded a youngest cluster of ages that ranged between 531 Ma and 475 Ma, with the youngest pair of analyses suggesting an intrusive age of 476 Ma. However, sample LHL0228 consists of a wide range of older Proterozoic ages, which were interpreted to have been inherited from the Cape River Beds from which the complex intruded (Henderson et al., 2020). The young cluster of Paleozoic ages are broadly synchronous with the ages obtained from the P16 migmatite sample in this study, and thus, synchronous with the early-Paleozoic, high-grade metamorphism and metamorphic zircon growth event. Therefore, we suggest that the < 1050 Ma ages in CRA2, and the Neoproterozoic-Paleozoic ages from LHL0228, may reflect partial to complete contamination of analyses by early-Paleozoic metamorphic zircon growth as discussed above.

8.2. Reworking of Proterozoic crust

The Hf isotope composition of zircon has proven an effective tool in tracking mantle melting episodes and crustal growth through time (Hawkesworth and Kemp, 2006; Belousova et al., 2010; Wang et al., 2012). The Hf isotopic evolution trends for samples of the P3 Intrusion, FHCC mylonite, and P16 migmatite are presented in Fig. 8. The Hf isotope evolution trend forms an array indicating reworking of Meso- and Paleoproterozoic crust (Fig. 8). Concordant, ~ 1200 Ma zircons from the P3 Intrusion contain a wide range of epsilon Hf compositions consistent with a mixed crustal, and mantle-derived signature. This signature is probably the result of crustal reworking of juvenile material produced during the ~ 1600 Ma and 2000 Ma mantle-melting episode, with lim-

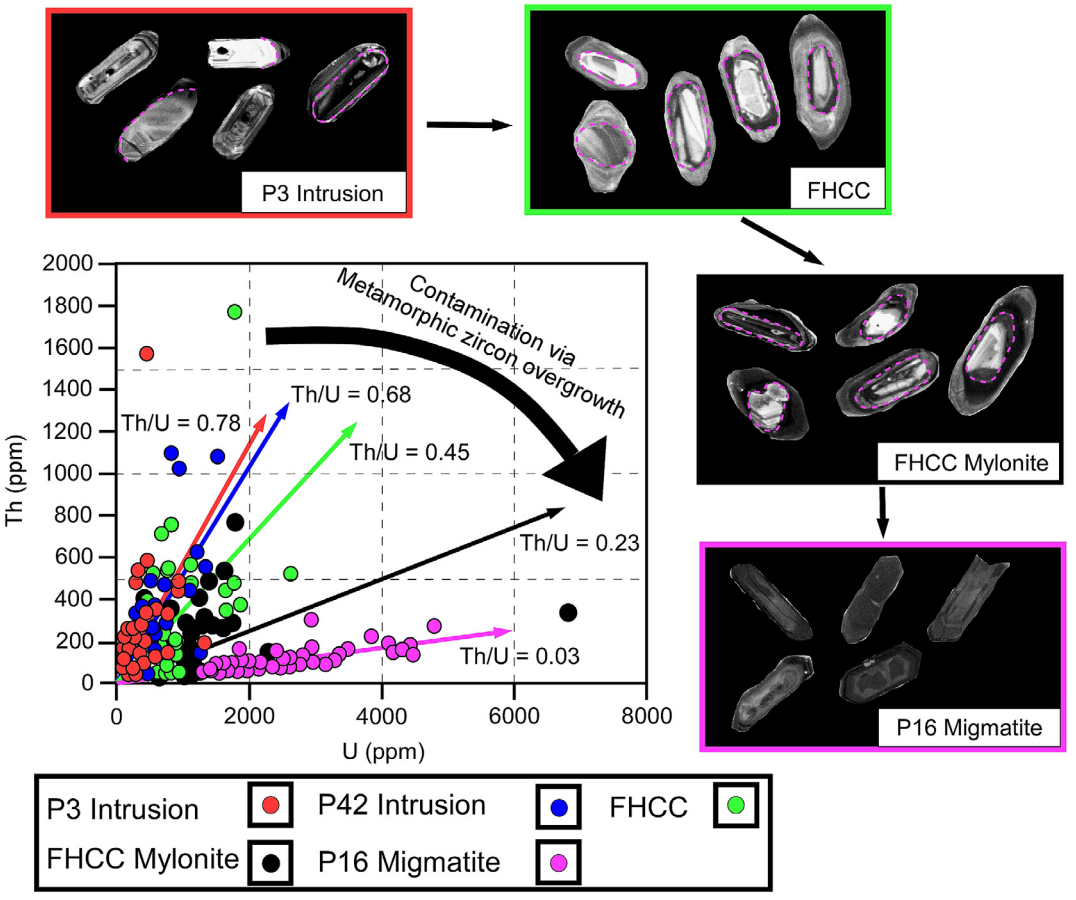

Fig. 6. Composite image illustrating the relationship between Th/U content in zircon, and the progressive increase in metamorphic zircon growth. The Th/U content of the P3, P42 and FHCC samples trends towards the Th/U content of the P16 migmatite. We interpret this trend as a product of analytical mixing of igneous and metamorphic generations of zircon. CL images reveal thick overgrowth zones have developed within zircons from the FHCC, consistent with their progressive reduction on Th/U content. Additionally, the overgrowth zones display similar luminescent properties to the metamorphic zircons from the P16 migmatite.

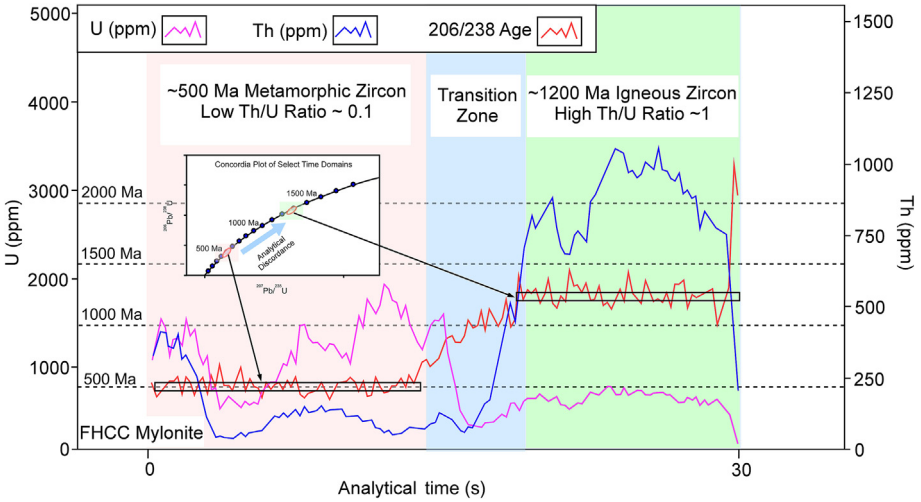

Fig. 7. Composite figure depicting the relationship between zircon chemistry (U, Th contents) and age generations (~500 Ma and ~ 1200 Ma) from a select analysis (P13E Grain 15) of the FHCC Mylonite. Inset concordia plot illustrates how selection bias influences the age determination, whilst demonstrating the discordance as a product of analytical mixing between two generations of zircon. ~ 1200 Ma zircon comprises high Th/U contents of ~ 1, typical of igneous zircon, whilst ~ 500 Ma zircon displays low Th/U contents of ~ 0.1, typical of metamorphic zircon. Separating both generations is a clear transition zone of analytical mixing between zircons generations (age) and chemistry (U, Th).

ited input from mantle material. The final reworking event was recorded by concordant, ~ 500 Ma metamorphic zircons from the P16 migmatite and FHCC granite. These zircons contain strongly negative epsilon Hf compositions, indicating that their source melts were not the product of mantle melting, but instead were derived from reworking of pre-existing crustal material produced

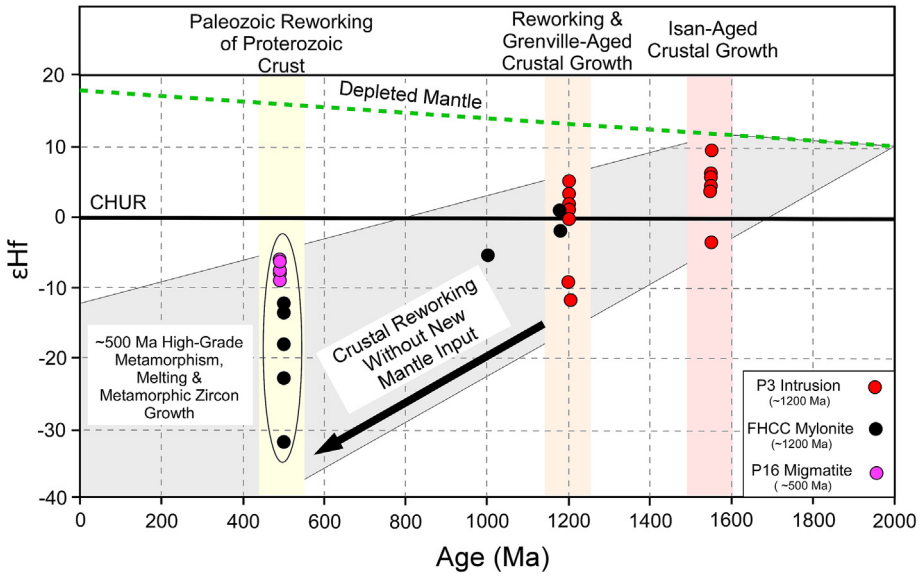

Fig. 8. Hf isotope compositions of zircon grains from the P3 Intrusion (red), FHCC Mylonite (black), and P16 migmatite (pink). Ablation sites were selected atop of previously analysed zircon grains which returned concordant U/Pb results. The Hf isotopic signatures are consistent with an initial episode of mantle-derived melting, concurrent with the widespread Isan Orogeny recorded by northeastern Australia during the Paleoproterozoic. This was followed by a Mesoproterozoic phase of mixed mantle melting and crustal reworking. Finally, an early-Palaeozoic, high-grade metamorphic event has been recorded by metamorphic zircon growth which contain Hf isotope compositions strongly reflective of crustal reworking without new mantle melt input.

during the ~ 1200 Ma and ~ 1600–2000 Ma crustal reworking and mantle melting events, respectively.

8.3. The tectonic setting of 1200 Ma intrusions

Major and trace element geochemistry and mineralogy can be used as tools to discriminate the tectonic setting of igneous rocks (Pearce et al., 1984; Barbarin, 1990; Frost and Frost, 2008). The P3 Intrusion and P42 Intrusion are calc-alkaline, metaluminous, hornblende-magnetite bearing, I-type granitoids (Chappell and White, 2001; Zandomeni et al., 2021). They contain negative Nb-Ta anomalies and moderate HREE fractionation consistent with a subduction-related setting (Pearce, 1982; Baier et al., 2008), and plot within the volcanic-arc discriminatory fields after Pearce et al. (1984). These chemical and mineralogical characteristics reflect a continental-arc setting for the emplacement of the P3 Intrusion and P42 Intrusion. The FHCC granite is a calc-alkaline, peraluminous, mica-rich, S-type granitoid. The two samples of the FHCC granite display contrasting HREE fractionation patterns, with the mylonite sample recording significant HREE depletion. We attribute the depletion of HREE in the mylonitic sample to reflect element mobility during mylonitization and subsequent concentrated fluid flow (Rolland et al., 2003; Beinlich et al., 2010). The chemical and mineralogical characteristics of the FHCC granite are also consistent with a volcanic-arc setting, and may represent collisional granites derived during crustal thickening and sediment anatexis (Clemens, 2003; Zhu et al., 2020).

8.4. The Oakvale Province

There is a consensus that the Tasmanides of eastern Australia developed in response to a protracted, Neoproterozoic-Paleozoic, westward dipping subduction system (Kemp et al., 2009; Glen, 2013; Rosenbaum, 2018). The ~ 1200 Ma, continental-arc magmatism documented in this study, predates the existence of this subduction system, and indicates that at least part of the Tasmanides record an earlier history. Furthermore, the ~ 1200 Ma arc must have developed atop of > 1200 Ma continental crust, suggesting the existence concealed basement terrane(s) along the southeastern margin of the North Australian Craton. We name this terrane the Oakvale Province, after the Oakvale Station from which the ~ 1200 Ma intrusions were discovered.

The positioning of the ~ 1200 Ma magmatism, southeast of the Cork Fault, likely indicates that the arc developed in response to a southeastward dipping subduction complex below an exotic terrane. This interpretation is consistent with a lack late-Mesoproterozoic geology craton-side of the Cork Fault, and the interpretations of seismic profiles across the Cork Fault by Korsch et al. (2012) and Korsch et al. (2024). This implies that the Cork Fault is a continental suture between the NAC and said exotic terrane, and that this boundary records Wilson-cycle style processes of subduction, ocean closure, and terrane collision (Buiter and Torsvik, 2014; Wilson et al., 2019). We present three possible scenarios (Figs. 9, 10 and 11) for the origin of the Oakvale Province, each of which is based upon an existing pre-Rodinia tectonic configuration.

Scenario one (Fig. 9) depicts the Oakvale Province as an exotic terrane, with no known affinity to other terranes. Many authors have proposed a connection between the NAC and Laurentia within the Nuna and Rodinia supercontinent configurations (Karlstrom et al., 2001; Betts et al., 2008; Kirscher et al., 2021). Nordsvan et al. (2018), Olierook et al. (2021) and Volante et al. (2022) have proposed that this connection is best recorded by the Georgetown Inlier, thought to be a relic piece of Laurentian crust. The NAC-Laurentia connection is depicted in Scenario one (Fig. 9) via the Georgetown Inlier, which was sutured together either prior-to, or during the late-Mesoproterozoic. At ~ 1200 Ma, an outboard subduction complex dips below the Oakvale Province (OP), and in response to Mesoproterozoic convergence, this subduction complex retreats northwestwards, and an ocean basin which separates the NAC and OP is progressively closed (Fig. 9A). This northwestward retreat transports the OP, towards Australia, until the ocean basin is completely closed and the Oakvale Province is sutured to Australia along the Cork Fault (Fig. 9B).

Some authors have proposed the Tarim Block to represent a missing link between Australia and Laurentia, and this is explored

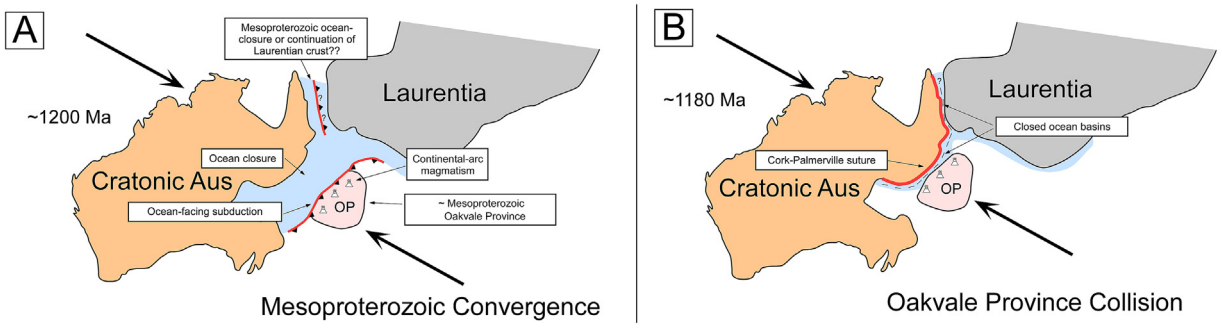

Fig. 9. Graphical depiction of Scenario One detailing the Mesoproterozoic evolution of the Oakvale Province as an exotic continental fragment. (A) An outboard, late-Mesoproterozoic, ocean-facing subduction complex develops below the Oakvale Province. (B) Protracted late-Mesoproterozoic convergence results in ocean closure, and migration of the Oakvale Province (and its continental arc) towards Australia. The Oakvale Province collides with Australia along the Cork Fault, which may represent a continuation of the Palmerville Fault.

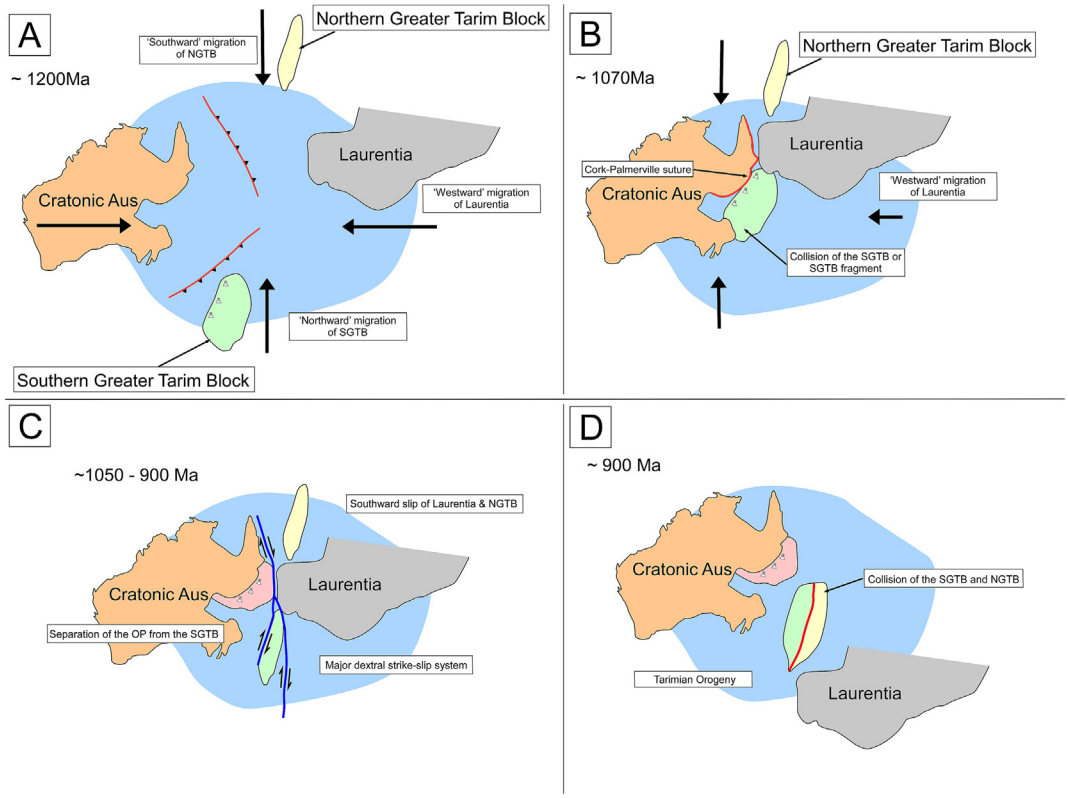

Fig. 10. Tectonic schematic depicting a possible link between the Oakvale Province and the Tarim Block. Model adapted from Wen et al. (2018). (A) At approximately 1200 Ma, eastward dipping subduction complexes facilitate the westward migration of Laurentia towards Australia, as well as continental arc magmatism within the Southern Greater Tarim Block (SGTB). (B) Laurentia and the SGTB collide with Australia. (C) Continuous convergence is accommodated by a major dextral strike slip system, which separates Laurentia and the SGTB from Australia and the Oakvale Province, respectively. (D) Ongoing south directed slip of the Northern Greater Tarim Block (NGTB) results in collision between the SGTB and NGTB, during the Tarimian Orogeny at ~ 900 Ma.

in scenario two (Wen et al., 2017, 2018). Prior to suturing and final assembly during the Tarimian Orogeny at ~ 900 Ma, the Tarim block was subdivided in to the Southern Greater Tarim Block (SGTB) and Northern Greater Tarim Block (NGTB) (Fig. 10A). Wen et al. (2018) proposed that during the mid-Mesoproterozoic, Laurentia collided approximately orthogonally with Australia (Fig. 10B). This collision event was proposed to have occurred within proximity of the SGTB and NGTB, and following major dextral, north–south oriented strike-slip, Australia and Laurentia were separated once more. By ~ 900 Ma, the southward slipping NGTB is proposed to have collided with the SGTB, suturing the terranes. It is possible that the Oakvale Province represents one of the SGTB terranes, which potentially collided with Australia (Fig. 10B). Following the proposed late-Mesoproterozoic mega-shearing event (Fig. 10C), the Oakvale Province may have remained sutured to Australia, whilst Laurentia and the remaining SGTB were separated. As proposed, continued strike-slip movement transported the NGTB and now detached SGTB.

The final scenario (Fig. 11) depicts the Oakvale Province originating as part of the Yangtze Craton, which some authors have proposed was in close proximity to eastern Australia and Cathaysia within the core of Rodinia during the Mesoproterozoic-Neoproterozoic (Li et al., 2002, 2008; Nesheim et al., 2012). As proposed in the previous models presented in this study, outboard subduction below the Yangtze Craton triggers ~ 1200 Ma continental-arc magmatism, and the northwestward transport of

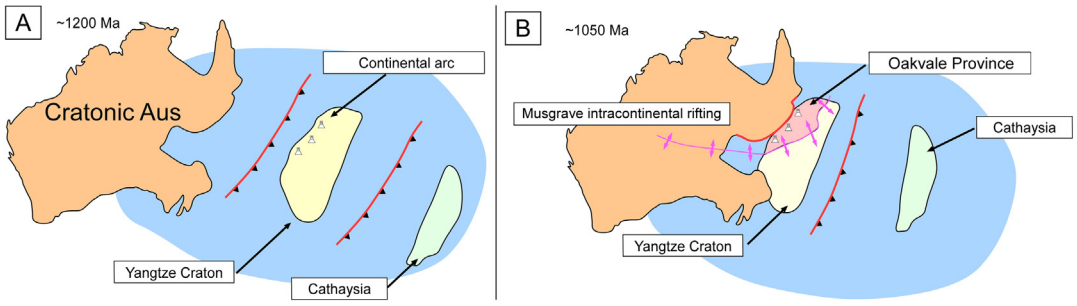

Fig. 11. Possible tectonic scenario involving collision of the Yangtze Craton. Positioning of the Yangtze craton after Li et al. (2008) and Nesheim et al. (2012). (A) Multiple outboard subduction complexes drive westward migration of the Yangtze Craton and Cathaysia towards Australia. (B) The Yangtze Craton collides with Australia, and at approximately 1050 Ma, is rifted from Australia. This event is synchronous with the Musgrave intracontinental rifting event (Evins et al., 2010). During this rifting event, the "greater" Yangtze Craton is split into the Yangtze Craton and Oakvale Province. The Oakvale Province remains sutured to Australia, whilst the Yangtze craton drifts towards Cathaysia. The Yangtze Craton and Cathaysia suture at ~ 1 Ga (Li et al., 2002).

the Yangtze Craton towards Australia (Fig. 11A). The Yangtze Craton then collides with Australia along the Cork Fault during the Mesoproterozoic, consistent with late-Mesoproterozoic metamorphism reported by Li et al. (2002) from the Yangtze Craton. Separation of the Yangtze Craton and Australia may be related to initiation of the Musgrave intracontinental rifting event (Ngaanyatjarra Rift) at ~ 1090–1040 Ma (Evins et al., 2010; Aitken et al., 2013; Howard et al., 2015). This event is synchronous with widespread, rift-related intracontinental magmatism documented by Lu et al. (2022) across the Yangtze Craton. During this proposed rifting event, the Oakvale Province remained docked to Australia, whilst the Yangtze Craton migrated offshore, eventually suturing to Cathaysia during the late-Mesoproterozoic and Neoproterozoic (Wang et al., 2007; Qiao et al., 2015; Cawood et al., 2018).

8.5. Challenges to "Missing Link" models

Scenarios two and three presented here are adapted from the "Missing Link" models first established by Li et al. (1995). The original model proposed that the Yangzte Craton (Yangtze-Cathaysia) was positioned between Australia and Laurentia within the core of Rodinia during the Late-Mesoproterozoic to early-Neoproterozoic times. This interpretation connects late-Mesoproterozoic tectonism through eastern Antarctica, central Australia, and the Yangtze Craton into a single mobile belt linked to the Grenville Orogeny (Li et al., 1995). Several adaptations to the model have been proposed (Li et al., 2008, 2013; Li and Evans, 2011) and more recently, the Tarim Block has been proposed as an alternative Missing Link between Australia and Laurentia (Wen et al., 2017, 2018). The Missing Link models involving south China have been challenged by Merdith et al. (2017) who argued that a viable mechanism would first need to be proposed to explain the complexity of flowlines, significant rotation of cratonised southern China, and rapid rates of rifting that were required to achieve the Missing-Link configuration. Merdith et al. (2017) also challenged the Tarim Block Missing Link models on the basis of inconsistencies in tectonic setting along northwestern Tarim during the late-Neoproterozoic.

As depicted in scenarios two and three (Figs. 10 and 11), an earlier separation of the Missing Link terrane from Australia may provide a solution to criticisms of Missing Link models. Separation of southern China from Australia in the late-Mesoproterozoic, contemporaneous with rifting in the Musgrave Province, may enable a more realistic rate of rifting along proposed rift path trajectories. Similarly, convergent tectonics and the emplacement of blueschists at ~ 750 Ma along margins of the Tarim Block (Yong et al., 2013) would no longer overlap with rifting given an earlier separation of the Tarim Block from Australia at ~ 900 Ma.

8.6. The source of late-Mesoproterozoic zircon

Neoproterozoic-Paleozoic metasedimentary successions across the Tasmanides commonly contain a pronounced, late-Mesoproterozoic (1.3 Ga – 1 Ga) detrital zircon signature. There is a general agreement regarding the source of late-Mesoproterozoic detritus, with most authors in support of a local source (Fergusson and Henderson, 2015; Purdy et al., 2016, 2018), probably from the Musgrave Province of central Australia (Wade et al., 2008; Smithies et al., 2010), or an eastward continuation of the province undercover. Weathering, erosion, and sedimentation of this source is thought to have happened during the 650–550 Ma Petermann Orogeny (Aitken et al., 2009), whereby voluminous late-Mesoproterozoic magmatic rocks were uplifted and eroded into the Centralian Super Basin, connected to the Thomson Orogen (Purdy et al., 2016). The Cape River Beds, which contain an almost unimodal late-Mesoproterozoic detrital zircon signature (Henderson et al., 2020), are crosscut by the ~ 1200 Ma intrusions documented in this study. Therefore, deposition of the Cape River Beds must have significantly predated the Petermann Orogeny. We instead propose that deposition of the Cape River Beds was broadly synchronous with the ~ 1200 Ma continental magmatism.

The extent of the Oakvale Province, and its relationship to the Thomson and Mossman Orogens, is difficult to ascertain, largely due to the Phanerozoic cover sequences (Murray and Kirkegaard, 1978; Habermehl, 2020) which hinder the geophysical response of the basement rocks across much of Queensland (Spampinato et al., 2015). However, there are some possible indications that Mesoproterozoic basement is widespread throughout North Queensland. For example, sedimentary sequences from the Iron Range Province, in far-north Queensland, record similar detrital zircon signatures to those in the Cape River Beds (Blewett et al., 1998; Blewett and Black, 1998). Furthermore, a basement terrane, termed the Brighton Downs Seismic Province, has been recently delineated within seismic profiling across the Cork Fault (Korsch et al., 2024). The Brighton Downs Seismic Province was interpreted to have been accreted to the NAC during Rodinia assembly, and is probably a buried equivalent of the Oakvale Province. Continuity of the Brighton Downs Seismic Province towards the Oakvale Province indicates a significant volume of late-Mesoproterozoic crust exists in north Queensland. The volume of late-Mesoproterozoic material in north Queensland, combined with a potential Musgravian source, would be more than capable of supplying the Tasmanides with enough detritus to produce the characteristic late-Mesoproterozoic detrital zircon signatures reported across eastern Australia.

8.7. Tectonic framework

The position of the Neoproterozoic rift margin, which facilitated the separation of Australia during the breakup of Rodinia, has yet to be fully resolved. Some authors have positioned the rift margin along the Tasman Line, which was thought to represent the easternmost extent of cratonic Australia (Li and Powell, 2001; Greene, 2010), whilst other authors position the margin further to the east (Direen and Crawford, 2003; Spampinato et al., 2015). We prefer the interpretation of Direen and Crawford (2003), in that the Tasman Line is a complex, disconnected boundary, which recorded a protracted history of various intricate processes along its extent. In north Queensland, we propose that the Tasman Line, and more specifically, the Cork Fault and Palmerville Fault systems, record Mesoproterozoic continental suturing, and potentially earlier, and later phases of intracontinental rifting. With the Oakvale Province and Brighton Downs Seismic Province positioned along the Cork Fault, we propose that rifting associated with the breakup of Rodinia, likely occurred further to the east, and along the margins of the Oakvale Province (Fig. 12).

As previously stated, the extent of the Oakvale Province, and thus the position of its margins, is undefined. However, its extent may be partly inferred by a semi-continuous, continent-scale belt of Paleozoic contractional deformation fabrics, which are clearly evident in regional magnetics (Poudjom Djomani et al., 2019). These fabrics, illustrated in Fig. 12 in green, extend throughout the northern Tasmanides (de Gromard, 2013; Nakamura and Milligan, 2015) and generally run parallel to the exposed margins of the Thomson Orogen (de Gromard, 2013; Abdullah et al., 2020; Dirks et al., 2021). It's possible that this orocline-like warping of the fabric formed in response to Paleozoic contractional deformation against concealed extensions of the Oakvale Province. Therefore, this orocline may provide an indication of the spatial extent of the Oakvale Province (Fig. 12). In this case, the Rodinia rift margin would be positioned accordingly along the eastern margin of the Oakvale Province (Fig. 12). Potential exposures of the rift margin may be preserved within the Anakie Inlier, Charters Towers Province, Greenvale Province, or Iron Range Province.

9. Conclusions

The Cape River Metamorphics in north Queensland contain ~ 1200 Ma intrusions of continental-arc affinity, which constrain the age of basement metasediments in the region to > 1200 Ma. This indicates the existence of Mesoproterozoic continental crust below the Neoproterozoic – Paleozoic Thomson Orogen. We have termed this basement terrane the Oakvale Province. The origin of the Oakvale Province is unknown, but we provide models which detail potential links to Laurentia, the Tarim Block, and the Yangtze Craton, during the transition from Nuna to Rodinia. We propose that the Tasman Line in northeast Queensland (Cork Fault) is not a rift margin, but instead, a Mesoproterozoic suture zone between the North Australian Craton and the Oakvale Province. We have repositioned the Neoproterozoic rift margin, associated with Rodinia breakup, to the eastern margin of the Oakvale Province. Paleozoic oroclinal bending along this margin potentially resulted from contractional deformation against competent, concealed, Proterozoic crust of the Oakvale Province.

CRediT authorship contribution statement

Alexander Edgar: Writing – review & editing, Writing – original draft, Visualization, Validation, Software, Resources, Project administration, Methodology, Investigation, Formal analysis, Data curation. **Ioan Sanislav:** Writing – review & editing, Supervision, Funding acquisition, Conceptualization. **Paul Dirks:** Writing – review & editing, Supervision, Funding acquisition.

Declaration of competing interest

The authors declare that they have no known competing financial interests or personal relationships that could have appeared to influence the work reported in this paper.

Acknowledgements

The Authors would like to thank the Geological Survey of Queensland for their funding of the research project through the

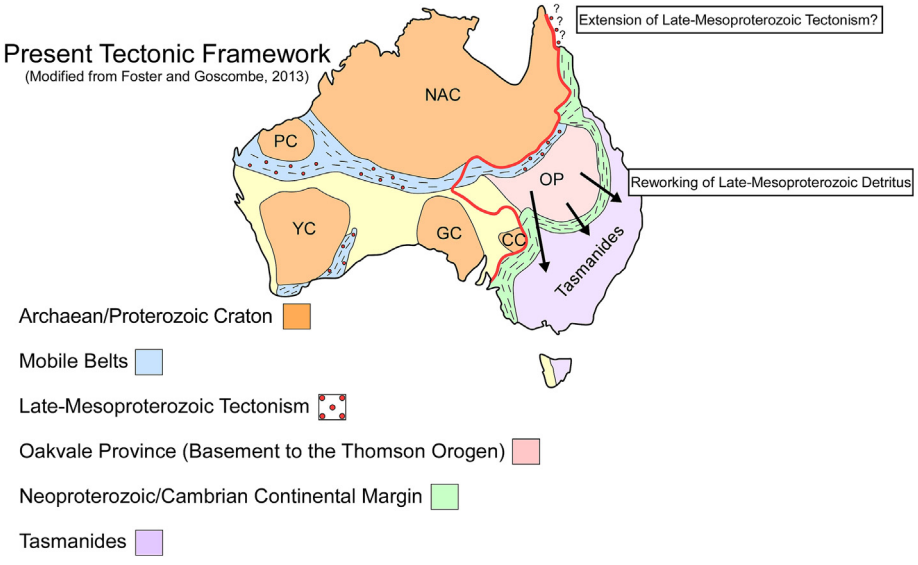

Fig. 12. Present-day tectonic framework of Australia, modified after Foster and Goscombe (2013). Grenville-aged orogens have been extended into northeast Queensland along the Cork Fault. The Thomson Orogen has been re-labelled as the Oakvale Province (OP), though its extent is unknown. Arrows depict the distribution of Grenville-aged detritus across eastern Australia. We propose that the Neoproterozoic rift margin, developed during Rodinia break-up, is positioned to the east of the Oakvale Province (pictured in green). This margin also shares a Neoproterozoic – Paleozoic history of convergence and deformation, recording the evolution of the Pacific-Gondwana margin.

New Economy Minerals Initiative (NEMI) program. The first Author would like to acknowledge the Australian Government Research Training Program Domestic Stipend Scholarship for financial support throughout this research, and the Economic Geology Research Centre (EGRU) at James Cook University for supporting this research. The Authors would like to thank the Editor, reviews from Alan Collins, and two anonymous reviewers for their constructive critiques which have resulted in a greatly improved manuscript. The Authors would like to thank Huiqing Huang from the Advanced Analytical Centre at James Cook University for technical support during LA-ICP-MS data collection and processing.

Appendix A. Supplementary data

Supplementary data to this article can be found online at https://doi.org/10.1016/j.gsf.2025.102017.

References

Abdullah, R., Shaanan, U., Lynn, K., Rosenbaum, G., 2020. Provenance and deformation history of the Eastern Thomson Orogen and implications for the Paleozoic evolution of the Tasmanides (Eastern Australia). Aust. J. Earth Sci. 67 (2), 153–173.
Aitken, A.R., Betts, P.G., 2008. High-resolution aeromagnetic data over central Australia assist Grenville-era (1300–1100 Ma) Rodinia reconstructions. Geophys. Res. Lett. 35 (1), L01306.
Aitken, A.R., Betts, P.G., Ailleres, L., 2009. The architecture, kinematics, and lithospheric processes of a compressional intraplate orogen occurring under Gondwana assembly: The Petermann orogeny, central Australia. Lithosphere 1 (6), 343–357.
Aitken, A.R., Smithies, R.H., Dentith, M.C., Joly, A., Evans, S., Howard, H.M., 2013. Magmatism-dominated intracontinental rifting in the Mesoproterozoic: The Ngaanyatjarra Rift, central Australia. Gondwana Res. 24 (3–4), 886–901.
Amelin, Y., Lee, D.-C., Halliday, A., 2000. Early-middle Archaean crustal evolution deduced from Lu-Hf and U-Pb isotopic studies of single zircon grains. Geochim. Cosmochim. Acta 64 (24), 4205–4225.
Ashwal, L.D., Tucker, R.D., Zinner, E.K., 1999. Slow cooling of deep crustal granulites and Pb-loss in zircon. Geochim. Cosmochim. Acta 63 (18), 2839–2851.
Baier, J., Audétat, A., Keppler, H., 2008. The origin of the negative niobium tantalum anomaly in subduction zone magmas. Earth Planet. Sci. Lett. 267 (1–2), 290–300.
Barbarin, B., 1990. Granitoids: main petrogenetic classifications in relation to origin and tectonic setting. Geol. J. 25 (3–4), 227–238.
Barton, M.D., Young, S., 2002. Non-pegmatitic deposits of beryllium: mineralogy, geology, phase equilibria and origin. Rev. Mineral. Geochem. 50 (1), 591–691.
Batchelor, R.A., Bowden, P., 1985. Petrogenetic interpretation of granitoid rock series using multicationic parameters. Chem. Geol. 48 (1–4), 43–55.
Beinlich, A., Klemd, R., John, T., Gao, J., 2010. Trace-element mobilization during Ca-metasomatism along a major fluid conduit: Eclogitization of blueschist as a consequence of fluid–rock interaction. Geochim. Cosmochim. Acta 74 (6), 1892–1922.
Belousova, E., Kostitsyn, Y., Griffin, W., Begg, G., O'reilly, S., Pearson, N., 2010. The growth of the continental crust: constraints from zircon Hf-isotope data. Lithos 119 (3–4), 457–466.
Betts, P., Armit, R., Stewart, J., Aitken, A., Ailleres, L., Donchak, P., Hutton, L., Withnall, I., Giles, D., 2016. Australia and nuna. Geol. Soc. London Spec. Pub. 424 (1), 47–81.
Betts, P.G., Giles, D., Schaefer, B.F., 2008. Comparing 1800–1600 Ma accretionary and basin processes in Australia and Laurentia: Possible geographic connections in Columbia. Precambrian Res. 166 (1–4), 81–92.
Blewett, R., Black, L., Sun, S., Knutson, J., Hutton, L., Bain, J., 1998. U-Pb zircon and Sm-Nd geochronology of the Mesoproterozoic of North Queensland: implications for a Rodinian connection with the Belt supergroup of North America. Precambrian Res. 89 (3–4), 101–127.
Blewett, R.S., Black, L.P., 1998. Structural and temporal framework of the Coen Region, north Queensland: Implications for major tectonothermal events in east and north Australia. Aust. J. Earth Sci. 45, 597–609.
Buiter, S.J., Torsvik, T.H., 2014. A review of Wilson Cycle plate margins: A role for mantle plumes in continental break-up along sutures? Gondwana Res. 26 (2), 627–653.
Cao, X., Collins, A.S., Pisarevsky, S., Flament, N., Li, S., Hasterok, D., Müller, R.D., 2024. Earth's tectonic and plate boundary evolution over 1.8 billion years. Geosci. Front. 15 (6), 101922.
Carson, C.J., Ague, J.J., Grove, M., Coath, C.D., Harrison, T.M., 2002. U–Pb isotopic behaviour of zircon during upper-amphibolite facies fluid infiltration in the Napier Complex, east Antarctica. Earth Planet. Sci. Lett. 199 (3–4), 287–310.
Cawood, P.A., 2005. Terra Australis Orogen: Rodinia breakup and development of the Pacific and Iapetus margins of Gondwana during the Neoproterozoic and Paleozoic. Earth-Sci. Rev. 69 (3–4), 249–279.
Cawood, P.A., Kroner, A., Collins, W.J., Kusky, T.M., Mooney, W.D., Windley, B.F., 2009. Accretionary orogens through Earth history. Geol. Soc. London Spec. Pub. 318, 1–36.
Cawood, P.A., Zhao, G., Yao, J., Wang, W., Xu, Y., Wang, Y., 2018. Reconstructing South China in Phanerozoic and Precambrian supercontinents. Earth-Sci. Rev. 186, 173–194.
Chappell, B.W., White, A.J., 2001. Two contrasting granite types: 25 years later. Aust. J. Earth Sci. 48 (4), 489–499.
Chen, R.-X., Zheng, Y.-F., Xie, L., 2010. Metamorphic growth and recrystallization of zircon: distinction by simultaneous in-situ analyses of trace elements, U–Th–Pb and Lu–Hf isotopes in zircons from eclogite-facies rocks in the Sulu orogen. Lithos 114 (1–2), 132–154.
Clark, D., Hensen, B., Kinny, P., 2000. Geochronological constraints for a two-stage history of the Albany–Fraser Orogen, Western Australia. Precambrian Res. 102 (3–4), 155–183.
Clemens, J., 2003. S-type granitic magmas—petrogenetic issues, models and evidence. Earth-Sci. Rev. 61 (1–2), 1–18.
de Gromard, R.Q., 2013. The significance of E–W structural trends for the Alice Springs Orogeny in the Charters Towers Province, North Queensland. Tectonophysics 587, 168–187.
Direen, N., Crawford, A., 2003. The Tasman Line: where is it, what is it, and is it Australia's Rodinian breakup boundary? Aust. J. Earth Sci. 50 (4), 491–502.
Dirks, H.N., Sanislav, I.V., Abu Sharib, A.S.A.A., 2021. Continuous convergence along the paleo-Pacific margin of Australia during the Early Paleozoic: Insights from the Running River Metamorphics, NE Queensland. Lithos 398–399, 106343.
Edgar, A., Sanislav, I., Dirks, P., 2023. The origin of mafic–ultramafic rocks and felsic plutons along the Clarke River suture zone: implications for porphyry exploration in the northern Tasmanides. Aust. J. Earth Sci. 70 (8), 1123–1138.
Edgar, A., Sanislav, I.V., Dirks, P.H., Spandler, C., 2022. Metamorphic diamond from the northeastern margin of Gondwana: Paradigm shifting implications for one of Earth's largest orogens. Sci. Adv. 8 (27), eabo2811.
Evins, P.M., Smithies, R.H., Howard, H.M., Kirkland, C.L., Wingate, M.T., Bodorkos, S., 2010. Devil in the detail: The 1150–1000 Ma magmatic and structural evolution of the Ngaanyatjarra Rift, west Musgrave Province, Central Australia. Precambrian Res. 183 (3), 572–588.
Fergusson, C.L., Carr, P.F., Fanning, C., Green, T., 2001. Proterozoic-Cambrian detrital zircon and monazite ages from the Anakie Inlier, central Queensland: Grenville and Pacific-Gondwana signatures. Aust. J. Earth Sci. 48 (6), 857–866.
Fergusson, C.L., Henderson, R.A., 2015. Early Palaeozoic continental growth in the Tasmanides of northeast Gondwana and its implications for Rodinia assembly and rifting. Gondwana Res. 28, 933–953.
Fergusson, C.L., Henderson, R.A., Fanning, C.M., Withnall, I.W., 2007a. Detrital zircon ages in Neoproterozoic to Ordovician siliciclastic rocks, northeastern Australia: implications for the tectonic history of the East Gondwana continental margin. J. Geol. Soc. 164 (1), 215–225.
Fergusson, C.L., Henderson, R.A., Lewthwaite, K.J., Phillips, D., Withnall, I.W., 2005. Structure of the Early Palaeozoic Cape River Metamorphics, Tasmanides of north Queensland: evaluation of the roles of convergent and extensional tectonics. Aust. J. Earth Sci. 52 (2), 261–277.
Fergusson, C.L., Henderson, R.A., Withnall, I.W., Fanning, C.M., Phillips, D., Lewthwaite, K.J., 2007b. Structural, metamorphic, and geochronological constraints on alternating compression and extension in the Early Paleozoic Gondwanan Pacific margin, northeastern Australia. Tectonics 26 (3), TC3008.
Flowers, R.M., Schmitt, A.K., Grove, M., 2010. Decoupling of U–Pb dates from chemical and crystallographic domains in granulite facies zircon. Chem. Geol. 270 (1–4), 20–30.
Foden, J., Elburg, M., Turner, S., Clark, C., Blades, M.L., Cox, G., Collins, A.S., Wolff, K., George, C., 2020. Cambro-Ordovician magmatism in the Delamerian orogeny: Implications for tectonic development of the southern Gondwanan margin. Gondwana Res. 81, 490–521.
Foster, D.A., Goscombe, B.D., 2013. Continental growth and recycling in convergent orogens with large turbidite fans on oceanic crust. Geosciences 3 (3), 354–388.
Frost, B.R., Frost, C.D., 2008. A geochemical classification for feldspathic igneous rocks. J. Petrol. 49 (11), 1955–1969.
Giacomini, F., Bomparola, R.M., Ghezzo, C., 2005. Petrology and geochronology of metabasites with eclogite facies relics from NE Sardinia: constraints for the Palaeozoic evolution of Southern Europe. Lithos 82 (1–2), 221–248.
Glen, R.A., 2005. The Tasmanides of eastern Australia. Geol. Soc. London Spec. Pub. 246, 23–96.
Glen, R.A., 2013. Refining accretionary orogen models for the Tasmanides of eastern Australia. Aust. J. Earth Sci. 60 (3), 315–370.
Greene, D.C., 2010. Neoproterozoic rifting in the southern Georgina Basin, central Australia: Implications for reconstructing Australia in Rodinia. Tectonics 29 (5), TC5010.
Greentree, M.R., Li, Z.-X., Li, X.-H., Wu, H., 2006. Late Mesoproterozoic to earliest Neoproterozoic basin record of the Sibao orogenesis in western South China and relationship to the assembly of Rodinia. Precambrian Res. 151 (1–2), 79–100.
Habermehl, M., 2020. The evolving understanding of the Great Artesian Basin (Australia), from discovery to current hydrogeological interpretations. Hydrogeol. J. 28 (1), 13–36.
Hawkesworth, C.J., Kemp, A., 2006. Using hafnium and oxygen isotopes in zircons to unravel the record of crustal evolution. Chem. Geol. 226 (3–4), 144–162.
Henderson, R.A., Fergusson, C.L., Withnall, I.W., 2020. Coeval basin formation, plutonism and metamorphism in the Northern Tasmanides: extensional Cambro-Ordovician tectonism of the Charters Towers Province. Aust. J. Earth Sci. 67 (5), 663–680.

Hölttä, P., Huhma, H., Mänttäri, I., Paavola, J., 2000. P–T–t development of Archaean granulites in Varpaisjärvi, Central Finland: II. Dating of high-grade metamorphism with the U–Pb and Sm–Nd methods. Lithos 50 (1–3), 121–136.
Howard, H., Smithies, R., Kirkland, C., Kelsey, D., Aitken, A., Wingate, M., De Gromard, R.Q., Spaggiari, C., Maier, W.D., 2015. The burning heart—the Proterozoic geology and geological evolution of the west Musgrave Region, central Australia. Gondwana Res. 27 (1), 64–94.
Karlstrom, K.E., Åhäll, K.-I., Harlan, S.S., Williams, M.L., McLelland, J., Geissman, J.W., 2001. Long-lived (1.8–1.0 Ga) convergent orogen in southern Laurentia, its extensions to Australia and Baltica, and implications for refining Rodinia. Precambrian Res. 111 (1–4), 5–30.
Kemp, A., Hawkesworth, C., Collins, W., Gray, C., Blevin, P., 2009. Isotopic evidence for rapid continental growth in an extensional accretionary orogen: The Tasmanides, eastern Australia. Earth Planet. Sci. Lett. 284 (3–4), 455–466.
Kirscher, U., Mitchell, R.N., Liu, Y., Nordsvan, A.R., Cox, G.M., Pisarevsky, S.A., Wang, C., Wu, L., Murphy, J.B., Li, Z.-X., 2021. Paleomagnetic constraints on the duration of the Australia-Laurentia connection in the core of the Nuna supercontinent. Geology 49 (2), 174–179.
Kooijman, E., Upadhyay, D., Mezger, K., Raith, M.M., Berndt, J., Srikantappa, C., 2011. Response of the U–Pb chronometer and trace elements in zircon to ultrahigh-temperature metamorphism: the Kadavur anorthosite complex, southern India. Chem. Geol. 290 (3–4), 177–188.
Korsch, R., Huston, D., Henderson, R., Blewett, R., Withnall, I., Fergusson, C.L., Collins, W.J., Saygin, E., Kositcin, N., Meixner, A., 2012. Crustal architecture and geodynamics of North Queensland, Australia: insights from deep seismic reflection profiling. Tectonophysics 572, 76–99.
Korsch, R.J., Doublier, M.P., Brown, D.D., Simpson, J.M., Cross, A.J., Costelloe, R.D., Jiang, W., 2024. Crustal architecture and tectonic development of western Queensland, Australia, based on deep seismic reflection profiling: Implications for Proterozoic continental assembly and dispersal. Tectonophysics 878, 230302.
Li, Z.-X., Bogdanova, S., Collins, A., Davidson, A., De Waele, B., Ernst, R., Fitzsimons, I., Fuck, R., Gladkochub, D., Jacobs, J., 2008. Assembly, configuration, and break-up history of Rodinia: a synthesis. Precambrian Res. 160 (1–2), 179–210.
Li, Z.-X., Evans, D.A., 2011. Late Neoproterozoic 40 intraplate rotation within Australia allows for a tighter-fitting and longer-lasting Rodinia. Geology 39 (1), 39–42.
Li, Z.-X., Evans, D.A., Halverson, G.P., 2013. Neoproterozoic glaciations in a revised global palaeogeography from the breakup of Rodinia to the assembly of Gondwanaland. Sediment. Geol. 294, 219–232.
Li, Z.-X., Li, X.-H., Zhou, H., Kinny, P.D., 2002. Grenvillian continental collision in south China: New SHRIMP U-Pb zircon results and implications for the configuration of Rodinia. Geology 30 (2), 163–166.
Li, Z.-X., Powell, C.M., 2001. An outline of the palaeogeographic evolution of the Australasian region since the beginning of the Neoproterozoic. Earth-Sci. Rev. 53 (3–4), 237–277.
Li, Z.-X., Wartho, J.-A., Occhipinti, S., Zhang, C.-L., Li, X.-H., Wang, J., Bao, C., 2007. Early history of the eastern Sibao Orogen (South China) during the assembly of Rodinia: new mica $^{40}Ar/^{39}Ar$ dating and SHRIMP U–Pb detrital zircon provenance constraints. Precambrian Res. 159 (1–2), 79–94.
Li, Z.-X., Zhang, L., Powell, C.M., 1995. South China in Rodinia: part of the missing link between Australia–East Antarctica and Laurentia? Geology 23 (5), 407–410.
Lloyd, J.C., Blades, M.L., Counts, J.W., Collins, A.S., Amos, K.J., Wade, B.P., Hall, J.W., Hore, S., Ball, A.L., Shahin, S., 2020. Neoproterozoic geochronology and provenance of the Adelaide Superbasin. Precambrian Res. 350, 105849.
Lloyd, J.C., Collins, A.S., Blades, M.L., Gilbert, S.E., Amos, K.J., 2022. Early evolution of the Adelaide Superbasin. Geosciences 12 (4), 154.
Lu, G.-M., Spencer, C.J., Deng, X., Tian, Y., Huang, B., Jiang, Y.-D., Wang, W., 2022. Mesoproterozoic magmatism redefines the tectonics and paleogeography of the SW Yangtze Block, China. Precambrian Res. 370, 106558.
McDonough, W.F., Sun, S.-S., 1995. The composition of the Earth. Chem. Geol. 120 (3–4), 223–253.
Merdith, A.S., Williams, S.E., Müller, R.D., Collins, A.S., 2017. Kinematic constraints on the Rodinia to Gondwana transition. Precambrian Res. 299, 132–150.
Mezger, K., Krogstad, E., 1997. Interpretation of discordant U-Pb zircon ages: An evaluation. J. Metamorph. Geol. 15 (1), 127–140.
Middlemost, E.A., 1994. Naming materials in the magma/igneous rock system. Earth-Sci. Rev. 37 (3–4), 215–224.
Murray, C., Kirkegaard, A., 1978. The Thomson Orogen of the Tasman orogenic zone. Tectonophysics 48 (3–4), 299–325.
Nakamura, A., Milligan, P.R., 2015. Total Magnetic Intensity (TMI) Grid of Australia 2015. Sixth Edition, Geoscience Australia.
Nesheim, T.O., Vervoort, J.D., McClelland, W.C., Gilotti, J.A., Lang, H.M., 2012. Mesoproterozoic syntectonic garnet within Belt Supergroup metamorphic tectonites: Evidence of Grenville-age metamorphism and deformation along northwest Laurentia. Lithos 134, 91–107.
Nordsvan, A.R., Collins, W.J., Li, Z.-X., Spencer, C.J., Pourteau, A., Withnall, I.W., Betts, P.G., Volante, S., 2018. Laurentian crust in northeast Australia: Implications for the assembly of the supercontinent Nuna. Geology 46 (3), 251–254.
Olierook, H.K., Affleck, R.G., Evans, N.J., Jourdan, F., Kirkland, C.L., Volante, S., Nordsvan, A.R., McInnes, B.I., McDonald, B., Mayers, C., 2021. Mineralization proximal to the final Nuna suture in northeastern Australia. Gondwana Res. 92, 54–71.
Pearce, J.A., 1982. Trace element characteristics of lavas from destructive plate boundaries: Orogenic andesites and related rocks. In: Thorpe, R.S. (Ed.), Andesites. Wiley, New York, pp. 525–548.
Pearce, J.A., Harris, N.B., Tindle, A.G., 1984. Trace element discrimination diagrams for the tectonic interpretation of granitic rocks. J. Petrol. 25 (4), 956–983.
Poudjom Djomani, Y., Minty, B. R. S., Hutchens, M., Lane, R. J. L., 2019. Total Magnetic Intensity (TMI) Grid of Australia 2019 - seventh edition - 80 m cell size. Commonwealth of Australia (Geosciences Australia), Australia. doi: 10.26186/5e9cf3f2c0f1d.
Pourteau, A., Smit, M.A., Li, Z.-X., Collins, W.J., Nordsvan, A.R., Volante, S., Li, J., 2018. 1.6 Ga crustal thickening along the final Nuna suture. Geology 46 (11), 959–962.
Powell, C.M., Preiss, W., Gatehouse, C., Krapez, B., Li, Z.-X., 1994. South Australian record of a Rodinian epicontinental basin and its mid-Neoproterozoic breakup (~ 700 Ma) to form the Palaeo-Pacific Ocean. Tectonophysics 237 (3–4), 113–140.
Preiss, W., 2000. The Adelaide Geosyncline of South Australia and its significance in Neoproterozoic continental reconstruction. Precambrian Res. 100 (1–3), 21–63.
Purdy, D., Hegarty, R., Doublier, M., 2018. Basement geology of the southern Thomson Orogen. Aust. J. Earth Sci. 65 (7–8), 893–916.
Purdy, D.J., Cross, A.J., Brown, D.D., Carr, P.A., Armstrong, R.A., 2016. New constraints on the origin and evolution of the Thomson Orogen and links with central Australia from isotopic studies of detrital zircons. Gondwana Res. 39, 41–56.
Qiao, L., Wang, Q., Li, C., 2015. The western segment of the suture between the Yangtze and Cathaysia blocks: Constraints from inherited and co-magmatic zircons from Permian S-type granitoids in Guangxi, South China. Terra Nova 27 (5), 392–398.
Rolland, Y., Cox, S., Boullier, A.-M., Pennacchioni, G., Mancktelow, N., 2003. Rare earth and trace element mobility in mid-crustal shear zones: insights from the Mont Blanc Massif (Western Alps). Earth Planet. Sci. Lett. 214 (1–2), 203–219.
Rosenbaum, G., 2018. The Tasmanides: Phanerozoic tectonic evolution of Eastern Australia. Annu. Rev. Earth Planet. Sci. 46, 291–325.
Ross, P.-S., Bédard, J.H., 2009. Magmatic affinity of modern and ancient subalkaline volcanic rocks determined from trace-element discriminant diagrams. Can. J. Earth Sci. 46 (11), 823–839.
Rubatto, D., 2017. Zircon: the metamorphic mineral. Rev. Mineral. Geochem. 83 (1), 261–295.
Sheppard, S., Rasmussen, B., Muhling, J., Farrell, T., Fletcher, I., 2007. Grenvillian-aged orogenesis in the Palaeoproterozoic Gascoyne Complex, Western Australia: 1030–950 Ma reworking of the Proterozoic Capricorn Orogen. J. Metamorph. Geol. 25 (4), 477–494.
Smithies, R., Howard, H., Evins, P., Kirkland, C., Kelsey, D., Hand, M., Wingate, M., Collins, A., Belousova, E., Allchurch, S., 2010. Geochemistry, geochronology, and petrogenesis of Mesoproterozoic felsic rocks in the west Musgrave Province, central Australia, and implications for the Mesoproterozoic tectonic evolution of the region. Geological Survey of Western Australia, Perth, WA.
Smits, R., Collins, W., Hand, M., Dutch, R., Payne, J., 2014. A Proterozoic Wilson cycle identified by Hf isotopes in central Australia: Implications for the assembly of Proterozoic Australia and Rodinia. Geology 42 (3), 231–234.
Spampinato, G.P., Betts, P.G., Ailleres, L., Armit, R.J., 2015. Early tectonic evolution of the Thomson Orogen in Queensland inferred from constrained magnetic and gravity data. Tectonophysics 651, 99–120.
Spencer, C.J., Kirkland, C.L., Taylor, R.J., 2016. Strategies towards statistically robust interpretations of in situ U–Pb zircon geochronology. Geosci. Front. 7 (4), 581–589.
Vervoort, J.D., Kemp, A.I., 2016. Clarifying the zircon Hf isotope record of crust–mantle evolution. Chem. Geol. 425, 65–75.
Volante, S., Collins, W., Barrote, V., Nordsvan, A., Pourteau, A., Li, Z.-X., Li, J., Beams, S., 2022. Spatio–temporal evolution of Mesoproterozoic magmatism in NE Australia: A hybrid tectonic model for final Nuna assembly. Precambrian Res. 372, 106602.
Volante, S., Collins, W., Pourteau, A., Li, Z.X., Li, J., Nordsvan, A., 2020a. Structural evolution of a 1.6 Ga orogeny related to the final assembly of the supercontinent Nuna: coupling of episodic and progressive deformation. Tectonics 39 (10), e2020TC006162.
Volante, S., Pourteau, A., Collins, W.J., Blereau, E., Li, Z.X., Smit, M., Evans, N.J., Nordsvan, A.R., Spencer, C.J., McDonald, B.J., 2020b. Multiple P–T–d–t paths reveal the evolution of the final Nuna assembly in northeast Australia. J. Metamorph. Geol. 38 (6), 593–627.
Wade, B., Kelsey, D., Hand, M., Barovich, K., 2008. The Musgrave Province: stitching north, west and south Australia. Precambrian Res. 166 (1–4), 370–386.
Wan, Y., Liu, D., Dong, C., Liu, S., Wang, S., Yang, E., 2011. U–Th–Pb behavior of zircons under high-grade metamorphic conditions: a case study of zircon dating of meta-diorite near Qixia, eastern Shandong. Geosci. Front. 2 (2), 137–146.
Wang, L., Johnston, S.T., Chen, N., Wang, H., Xia, B., He, C., Ma, J., 2021. Late Mesoproterozoic low-P/T–type metamorphism in the North Wulan terrane: Implications for the assembly of Rodinia. GSA Bulletin 133 (11–12), 2243–2265.
Wang, X.-C., Li, X.-H., Li, Z.-X., Li, Q.-L., Tang, G.-Q., Gao, Y.-Y., Zhang, Q.-R., Liu, Y., 2012. Episodic Precambrian crust growth: evidence from U–Pb ages and Hf–O isotopes of zircon in the Nanhua Basin, central South China. Precambrian Res. 222, 386–403.
Wang, X.-L., Zhou, J.-C., Griffin, W. a., Wang, R.-C., Qiu, J.-S., O'reilly, S., Xu, X., Liu, X.-M., Zhang, G.-L., 2007. Detrital zircon geochronology of Precambrian basement sequences in the Jiangnan orogen: dating the assembly of the Yangtze and Cathaysia Blocks. Precambrian Res. 159(1-2), 117-131.
Wen, B., Evans, D.A., Li, Y.-X., 2017. Neoproterozoic paleogeography of the Tarim Block: An extended or alternative "missing-link" model for Rodinia? Earth Planet. Sci. Lett. 458, 92–106.

Wen, B., Evans, D.A., Wang, C., Li, Y.-X., Jing, X., 2018. A positive test for the Greater Tarim Block at the heart of Rodinia: Mega-dextral suturing of supercontinent assembly. Geology 46 (8), 687–690.
Wilson, R.W., Houseman, G.A., Buiter, S., McCaffrey, K.J., Doré, A.G., 2019. Fifty years of the Wilson Cycle concept in plate tectonics: an overview. Geol. Soc. London Spec. Pub. 470 (1), 1–17.
Yakymchuk, C., Kirkland, C.L., Clark, C., 2018. Th/U ratios in metamorphic zircon. J. Metamorph. Geol. 36 (6), 715–737.
Yang, B., Collins, A., Blades, M., Jourdan, F., 2023. Orogens and detritus: unravelling the Mesoproterozoic tectonic geography of northern Australia through coupled detrital thermo-and geo-chronometers. Aust. J. Earth Sci., 1–19
Yong, W., Zhang, L., Hall, C., Mukasa, S., Essene, E., 2013. The $^{40}Ar/^{39}Ar$ and Rb–Sr chronology of the Precambrian Aksu blueschists in western China. J. Asian Earth Sci. 63, 197–205.
Zandomeni, P.S., Moreno, J.A., Verdecchia, S.O., Baldo, E.G., Dahlquist, J.A., Morales Camera, M.M., Balbis, C., Benítez, M., Serra-Varela, S., Lembo Wuest, C.I., 2021. Crystallization conditions and petrogenetic characterization of metaluminous to peraluminous calc-alkaline orogenic granitoids from mineralogical systematics: the case of the Cambrian magmatism from the Sierra de Guasayán (Argentina). Minerals 11 (2), 166.
Zhu, Z., Campbell, I.H., Allen, C.M., Burnham, A.D., 2020. S-type granites: Their origin and distribution through time as determined from detrital zircons. Earth Planet. Sci. Lett. 536, 116140.